

1
2 **A comparison study between CMAQ-simulated and OMI-**
3 **retrieved NO₂ columns over East Asia for evaluation of**
4 **NO_x emission fluxes of INTEX-B, CAPSS, and REAS**
5 **inventories**
6
7

8 **K. M. Han¹, S. Lee¹, L. S. Chang², and, C. H. Song^{1,*}**
9

10
11
12
13 **Shortened title:** Tropospheric NO₂ columns over East Asia
14
15

- 16 1. School of Environmental Science and Engineering, Gwangju Institute of Science and
17 Technology (GIST), Gwangju, Korea, and also at Advanced Environmental Monitoring
18 Research Center (ADEMRC), Gwangju Institute of Science and Technology (GIST), Gwangju,
19 500-712, Korea
20 2. Air Quality Monitoring and Forecasting Center, National Institute of Environmental Research
21 (NIER), Incheon, 404-708, Korea
22
23
24
25
26
27
28
29
30

31
32 *** Corresponding author:** Phone) +82-062-715-3276; Fax) +82-062-715-3404
33 Email) chsong@gist.ac.kr
34
35
36
37
38
39
40

(For submission to **Atmospheric Chemistry & Physics**)

41 **Abstract**

42 Comparison between the CMAQ-calculated and OMI-retrieved tropospheric NO₂ columns
43 was carried out for 2006 over East Asia (100°-150°E; 20°-50°N) to evaluate the bottom-up
44 NO_x emission fluxes of INTEX-B, CAPSS, and REAS v1.11 inventories. The three emission
45 inventories were applied to the CMAQ model simulations for the countries of China, Korea,
46 and Japan, respectively. For the direct comparison between the two NO₂ columns, the
47 averaging kernels (AKs) obtained from the Royal Netherlands Meteorological Institute
48 (KNMI)/DOMINO v2.0 daily product were applied to the CMAQ-simulated data. The
49 analysis showed that the two tropospheric NO₂ columns from the CMAQ model simulations
50 and OMI observations ($\Omega_{\text{CMAQ,AK}}$ and Ω_{OMI}) had good spatial and seasonal correlation, with
51 correlation coefficients ranging from 0.71 to 0.96. In addition, the normalized mean errors
52 (NMEs) between the $\Omega_{\text{CMAQ,AK}}$ and Ω_{OMI} were found to range from ~40% to ~63%. The
53 $\Omega_{\text{CMAQ,AK}}$ were, on annual average, ~28% smaller (in terms of the NMEs) than the Ω_{OMI} ,
54 indicating that the NO_x emissions used were possibly underestimated in East Asia. Large
55 absolute differences between the $\Omega_{\text{CMAQ,AK}}$ and Ω_{OMI} were found, particularly over Central
56 East China (CEC) during winter (annual averaged mean error of $\sim 4.51 \times 10^{15}$ molecules cm⁻²).
57 Although such differences between the $\Omega_{\text{CMAQ,AK}}$ and Ω_{OMI} are likely caused by the errors and
58 biases in the NO_x emissions used in the CMAQ model simulations, it can be rather difficult to
59 quantitatively relate the differences to the accuracy of the NO_x emissions, because there are
60 also several uncertain factors in the CMAQ model, satellite-retrieved NO₂ columns and AK
61 products, and NO_x and other trace gas emissions. **In this context**, three uncertain factors were
62 selected and analyzed with sensitivity runs (monthly variations in NO_x emissions; influences
63 of different NO_x emission fluxes; and reaction probability of N₂O₅ radicals). Other uncertain
64 or possible influential factors were also discussed to suggest future direction of the study.

65 **Keywords:** Tropospheric NO₂ columns; Averaging Kernels; OMI sensor; CMAQ model;

1. Introduction

69 There has been growing public concern about serious smog events in East Asia due to
70 large amounts of anthropogenic pollutants in the atmosphere. Among the pollutants, nitrogen
71 oxides ($\text{NO}_x \cong \text{NO} + \text{NO}_2$) play a key role in tropospheric chemistry, such as ozone and
72 secondary aerosol formation. Also, in global climate change, atmospheric NO_x is believed to
73 make indirect negative contributions to radiative forcing in the atmosphere (Wild et al., 2001).
74 For example, secondary nitrates (NO_3^-) formed via the condensation of atmospheric HNO₃,
75 NO₃, and N₂O₅ into particles contribute, on average, 30.7% to aerosol direct radiative forcing
76 (ADRF) in East Asia during the winter season, which cannot be ignored in the estimation of
77 direct radiative forcing in East Asia (Park et al., 2014). HNO₃ formation via the reaction of
78 OH + NO₂ during the daytime and heterogeneous nitrate formation via the condensation of
79 N₂O₅ onto atmospheric particles during the nighttime are believed to be the main chemical
80 and physico-chemical processes removing NO_x from the atmosphere (McConnell and
81 McElroy, 1973; Platt et al., 1984; Dentener and Crutzen, 1993; Brown et al., 2006; Han and
82 Song, 2012).

83 Recently, several studies have reported annual increases in NO_x emissions in China
84 (Zhang et al., 2007; Zhang et al., 2009; Kurokawa et al., 2013). For example, according to the
85 Greenhouse gas and Air pollution INteractions and Synergies (GAINS) model simulations,
86 China makes the largest contribution to global NO_x emissions, and its contribution was
87 estimated to be 25% for 2010 (Cofala et al., 2012). Also, when several emissions scenarios
88 are applied to the GAINS simulations, the contribution of China is estimated to increase, to
89 ~29% in the years between 2015 and 2035 (Cofala et al., 2012). However, large uncertainty in
90 bottom-up NO_x emissions over East Asia has been reported (e.g. Streets et al., 2003; Zhang et

91 al., 2007; Klimont et al., 2009; Xing et al., 2011).

92 In the meantime, several studies have also reported rapid increases in atmospheric
93 NO₂ columns over China, based on Global Ozone Monitoring Experiment (GOME), Ozone
94 Monitoring Instrument (OMI), and SCanning Imaging Absorption spectroMeter for
95 Atmospheric CartographY (SCIAMACHY) observations (Richter et al., 2005; van der A et
96 al., 2006; Schneider and van der A, 2012; Hilboll et al., 2013; Itahashi et al., 2014). These
97 satellite observations have provided useful global/regional information on the spatial
98 distributions of NO₂ columns, and have also been used to investigate the accuracy of the
99 global and regional NO_x emissions (e.g. Martin et al., 2006; Uno et al., 2007; Wang et al.,
100 2007; Han et al., 2009).

101 However, these satellite observations are not “real” or “true” values, having different
102 vertical sensitivities at different altitudes in the atmosphere. To consider this vertical
103 sensitivity of the satellite observations, averaging kernels (AKs) should be introduced into
104 comparison studies between chemistry-transport model (CTM)-simulated and satellite-
105 retrieved tropospheric NO₂ columns (hereafter, denoted as Ω). The introduction of AKs could
106 correct the large systematic errors typically caused by assumed (or unrealistic) NO₂ vertical
107 profiles used in the retrieval process of the NO₂ columns (Rodgers, 2000; Eskes and Boersma,
108 2003). In particular, Eskes and Boersma (2003) reported that the use of AKs is crucial in
109 interpreting the retrieved Ω , because of the low sensitivity of satellite observations of NO₂
110 near the surface areas.

111 In this context, several studies have used AKs to evaluate the surface NO_x emissions
112 over several regions (e.g. Herron-Thorpe et al., 2010; Lamsal et al., 2010; Huijnen et al., 2010;
113 Ghude et al., 2013; Zyrichidou et al., 2013). The previous studies conducted by Han et al.
114 (2009; 2011) also compared the CTM-calculated tropospheric NO₂ columns with GOME-
115 retrieved tropospheric NO₂ columns to evaluate the bottom-up NO_x emissions over East Asia,

116 but without using the AKs. Based on the comparison, Han et al. (2011) concluded that the
117 bottom-up NO_x emissions used in CTM simulations over East Asia may be overestimated.
118 However, such comparison without the application of AKs is like comparing apples with
119 oranges, and is unreasonable. Therefore, one of the main objectives of this study was to
120 correct our previous conclusions, using the state-of-the-science knowledge and methods,
121 including the application of AKs to the CTM simulations. In this study, we intended to
122 evaluate three bottom-up NO_x emissions of INTEX-B, CAPSS, and REAS v1.11 inventories
123 in East Asia, using OMI-retrieved tropospheric NO₂ columns (Ω_{OMI}) from KNMI/DOMINO
124 v2.0 daily products and the CTM-calculated tropospheric NO₂ columns (Ω_{CTM}). To conduct
125 this investigation, the AKs obtained from the KNMI algorithm were applied, and then direct
126 comparison of the $\Omega_{\text{CTM,AK}}$ with Ω_{OMI} was carried out (refer to Sect. 3.1).

127 However, evaluation of the bottom-up NO_x emissions via comparison between
128 $\Omega_{\text{CTM,AK}}$ and Ω_{OMI} may be hampered by many uncertain factors such as: (i) uncertain temporal
129 variations in NO_x emissions in East Asia; (ii) uncertainty in meteorological fields; (iii)
130 uncertain or missing photo-chemistries in the CTM; and (iv) errors in the retrieved NO₂
131 columns and AKs. Because of these errors and uncertainties, it can sometimes be difficult to
132 directly and quantitatively relate the differences between the $\Omega_{\text{CMAQ,AK}}$ and Ω_{OMI} to the
133 accuracy of the NO_x emissions in East Asia. Some of these issues are therefore explored with
134 several sensitivity analyses, and other factors are also discussed in Sect. 3.2.

135

136 **2. Experimental Methods**

137 **2.1 Modeling descriptions**

138 First, for the CTM simulations, the US EPA/Models-3 CMAQ (Community Multi-
139 scale Air Quality) v4.7.1 model was used (Byun and Schere, 2006). To drive CMAQ model
140 simulations, two main drivers are needed: (i) meteorological fields and (ii) emission fields.

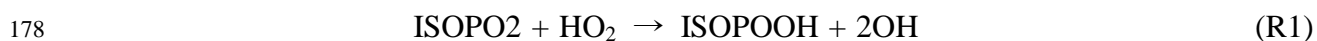
141 For the former, PSU/NCAR MM5 (Pennsylvania state University/National Center for
142 Atmospheric Research Meso-scale Model 5) v3.7.1 was used with National Centers for
143 Environmental Prediction (NCEP) reanalyzed data sets (Stauffer and Seaman, 1990; 1994).
144 To prepare more accurate meteorological fields, four-dimensional data assimilation (FDDA)
145 using QuickSCAT 10-m wind data sets was also carried out. For the latter, three
146 anthropogenic emission inventories were used: INTEX-B (Intercontinental Chemical
147 Transport Experiment-Phase B, Zhang et al., 2009), CAPSS (Clean Air Policy Support
148 System, Hong et al., 2008), and REAS v1.11 (Regional Emission Inventory in Asia, Ohara et
149 al., 2007) emission inventories for the year 2006. Annual $0.5^{\circ} \times 0.5^{\circ}$ -resolved INTEX-B and
150 REAS v1.11 emissions were interpolated into the CMAQ grid cells in China and Japan,
151 respectively. For biogenic emissions, the MEGAN-ECMWF (Model of Emissions of Gases
152 and Aerosols from Nature–European Center for Medium-Range Weather Forecasts) inventory
153 was obtained from the official website, at <http://tropo.aeronomie.be/models/isoprene.htm>
154 (Müller et al., 2008). Biogenic emissions are an important factor during the summer, even in
155 this type of NO_x study, because the mixing ratios of biogenic species can influence the NO_2 -
156 to- NO ratios via changing the levels of HO_x and RO_2 radicals (Horowitz et al., 2007; Han et
157 al., 2009). The accuracy of the biogenic emissions used in this study was also evaluated over
158 the same domain, East Asia, in our previous study (Han et al., 2013).

159 Table 1 summarizes base-case simulation and several sensitivity runs for this study.
160 For the base-case simulation, monthly variations of the anthropogenic NO_x emissions from
161 Zhang et al. (2009) were considered for China, while those from Han et al. (2009) were used
162 for Korea and Japan. The monthly factors were applied to the sectors of power generation,
163 residential areas, industry, and transportation. As shown in Fig. 1, data on several monthly
164 variations in NO_x emissions over China were available. Among them, two representative and
165 extreme monthly variations were chosen in this study, which were explored and discussed in

166 Sect. 3.2.1.

167 The modeling period was from January 1 to December 31, 2006. In this study, 2006
168 was chosen because the INTEX-B inventory was compiled for this year (the REAS v1.11 and
169 CAPSS inventories were also chosen for 2006). The horizontal domain covers from 100°E to
170 150°E and from 20°N to 50°N with a grid-resolution of 30 km × 30 km. The vertical domain
171 covers from 1000 hPa to 118 hPa with 14 terrain following σ -coordinates. For considering
172 aerosol dynamics and thermodynamics, the aerosol module of AERO4 was selected
173 (Binkowski and Roselle, 2003).

174 For the consideration of gas-phase chemistry, the SAPRAC-99 (Statewide Air
175 Pollution Research Center-99) mechanism was selected (Carter, 2000). Then, to consider
176 unknown OH radical processes (Lelieveld et al., 2008), the SAPRAC-99 mechanism was
177 modified partly, based on the work of Butler et al. (2008) in the following way (R1):



179 Here, ISOPO₂ and ISOPOOH represent isoprene-derived peroxy radical and peroxide,
180 respectively. Other schemes used in the CMAQ model simulations were the global mass-
181 conserving scheme (YAMO) for horizontal and vertical advection (Yamartino, 1993), the
182 asymmetric convective model (ACM) algorithm for convective cloud mixing, and ACM
183 (ver. 2) for vertical diffusion (Pleim, 2007).

184 In the CMAQ modeling, initial conditions (ICs) were prepared from 1 week-long
185 spin-up model simulations, and boundary conditions (BCs) were obtained from global CTM
186 simulations, MOZART (Model for OZone And Related chemical Tracers) (Emmons et al.,
187 2010). The MOZART model simulation data for the BCs were obtained from
188 <http://www.acd.ucar.edu/wrf-chem/mozart.shtml>. Other details about the model setup were
189 reported by Han et al. (2013).

190 For synchronization with the Ω_{OMI} , the Ω_{CMAQ} data were collected and then averaged

191 between 13:00 and 14:00 local time (LT), because the OMI sensor scans the atmosphere over
192 East Asia approximately at 13:45 LT. For further detailed analyses, eight highly-populated
193 focus regions were defined in this study, and are presented in Fig. 2.

194

195 **2.2 OMI-retrieved NO₂ columns and AKs**

196 The OMI instrument on board the NASA/EOS–Aura satellite, a nadir-viewing
197 imaging spectrometer, provides information on the properties of aerosols and clouds as well
198 as global levels of atmospheric species such as ozone, NO₂, SO₂, OClO, BrO, and HCHO on
199 a daily basis via observing backscattered UV-VIS radiances from 270 to 550 nm (Levelt et al.,
200 2006). Two-dimensional charge-coupled device (CCD) detectors equipped in the OMI
201 instrument observe the atmosphere with a spatial resolution of 13 km × 24 km at the nadir.
202 CCD1 covers the UV channel of 270-310 nm and 310-365 nm. The visible channel, ranging
203 from 365 to 500 nm, is covered by CCD2 to observe NO₂.

204 In this study, daily levels of OMI-retrieved tropospheric NO₂ columns from
205 KNMI/DOMINO v2.0 products were used (Boersma et al., 2007; 2011a). The
206 KNMI/DOMINO v2.0 algorithm (hereafter, KNMI algorithm) for retrieving the tropospheric
207 NO₂ columns from the OMI radiance data proceeds in the following sequence. First, a slant
208 NO₂ column density was determined from spectral fitting, using the differential optical
209 absorption spectroscopy (DOAS) method. Second, the stratospheric NO₂ contribution was
210 removed by subtracting the stratospheric portions of slant NO₂ columns from the total slant
211 NO₂ columns. The stratospheric NO₂ slant columns were calculated by data assimilation of
212 OMI-observed slant NO₂ columns in the global CTM (TM4) (Boersma et al., 2007). Finally,
213 the tropospheric slant NO₂ columns were converted into vertical NO₂ columns, using the air
214 mass factor (AMF), defined as the ratio of the measured slant column to the vertical column.
215 This AMF is a function of several factors, such as the satellite viewing geometry, surface

216 albedo, surface pressure, and vertical distributions of clouds, aerosols, and trace gases.

217 In this study, to reduce retrieval errors, measured scenes with surface albedo values
218 larger than 0.3 were excluded, as suggested by Boersma et al. (2011b). The surface albedo
219 data was obtained from the OMI observations (Kleipool et al., 2008). Also, observed pixels
220 with cloud radiance fractions (CRF) larger than 50% were filtered out, which are
221 approximately equivalent to cloud fractions (CF) smaller than 20% (van der A et al., 2006).
222 Thus, OMI-retrieved tropospheric NO₂ columns under almost “cloud-free” conditions were
223 used in this study.

224 Errors in the retrieval of the Ω_{OMI} can mainly be caused by calculations of the AMFs.
225 Boersma et al. (2011a) reported that errors of the Ω_{OMI} mostly due to calculations of the
226 AMFs in KNMI/DOMINO v2.0 products were approximated to be $\sim 1.0 \times 10^{15}$ molecules cm⁻²,
227 with a relative error of 25%. The other errors in the products were from the spectral fitting
228 ($\sim 0.7 \times 10^{15}$ molecules cm⁻²) and the stratospheric slant column ($\sim 0.25 \times 10^{15}$ molecules cm⁻²).

229 The AKs were also applied to the CMAQ model simulations. The AKs are
230 analytically expressed in Eq. (1) (Rodgers, 2000; Eskes and Boersma, 2003):

$$\begin{aligned} AK &= G_y K_x \\ &= \frac{\partial R}{\partial y} \frac{\partial F}{\partial x} \\ &= \frac{\partial \hat{x}}{\partial x} \end{aligned} \quad (1)$$

232 where G_y and K_x represent the sensitivities of the retrieval (R) to the measurement (y) and the
233 forward model (F) to the state (x), respectively. Also, K_x is known as a weighting function or
234 Jacobian matrix. Thus, as shown in Eq. (1), the AKs represent the sensitivity of the retrieved
235 quantities (here, vertical NO₂ column, \hat{x}) to the true atmospheric state (x). Using the AKs, the
236 retrieved quantity (\hat{x}) can be expressed by Eq. (2):

$$\hat{x} - \hat{x}_a = AK(x - x_a) + \varepsilon \quad (2)$$

238 where x_a and ε represent *a priori* estimate and total error in measured signal relative to the
239 forward model, respectively. Information on the AKs and retrieved quantity are included in
240 the daily KNMI products (http://www.temis.nl/airpollution/no2col/no2regioomi_v2.php).

241 Fig. 3 presents the vertical distributions of the seasonally-averaged AKs retrieved
242 from the KNMI algorithms over Central East China (CEC) and other regions (defined in Fig.
243 2). As shown in Fig. 3, the AKs are strongly altitude-dependent in the troposphere. For
244 example, near the surface, the AKs are smaller than unity, ranging between 0.2 and 0.7 (based
245 on seasonal averaged values). In contrast, in the upper troposphere, the AKs are larger than
246 unity, ranging between 1.1 and 2.1 (an AK of unity means that the OMI instruments can
247 directly measure the true NO₂ column densities). Additionally, the AKs are generally lower in
248 warm seasons than in cold seasons. These low values in the AKs during the summer are
249 probably related to low surface albedos, low concentrations of aerosols, and large uncertainty
250 in cloud retrieval during the summer (Eskes and Boersma, 2003).

251 Fig. 4 illustrates the main procedures of the comparison study. Once the CMAQ
252 model simulations were done, all the vertically-resolved NO₂ mixing ratios were interpolated
253 to the OMI footprints on a daily basis since the AKs are defined for the OMI footprints.
254 Interpolating AKs to model grid cells is not recommended because the AKs are sometimes
255 sensitive to changes on small spatial scales (Boersma et al., 2011b). After this, the AKs under
256 almost cloud-free conditions were applied to the NO₂ mixing ratios at different layers, and
257 were then integrated from surface to tropopause in order to calculate $\Omega_{\text{CMAQ,AK}}$. Meanwhile,
258 the tropospheric NO₂ columns were retrieved from the OMI observations via the KNMI
259 algorithms. A direct comparison study was then made between the two Ω products (i.e. Ω_{OMI}
260 vs. $\Omega_{\text{CMAQ,AK}}$).

261 For the purpose of this study, the seasonal average values of Ω_{OMI} and $\Omega_{\text{CMAQ,AK}}$ were
262 calculated (in case of the $\Omega_{\text{CMAQ,AK}}$, daily AK applications were first conducted and then

263 seasonal average values were calculated). Seasonal averaging was carried out to reduce the
264 “random errors” in the NO₂ retrieval process typically caused by instrument signal noise,
265 fitting errors, and uncertainty in cloud information. It has been suggested and demonstrated
266 that the random errors can be reduced by both temporal and/or spatial averaging (Fioletov et
267 al., 2002; Monaghan et al., 2006; Johnson et al., 2007; Richter et al., 2011; Clarisse et al.,
268 2013).

269 On the other hand, the application of AKs can reduce “smoothing errors” in the NO₂
270 retrieval process, which are mainly caused by bias in the *a priori* vertical NO₂ profiles. As
271 mentioned previously, TM4-derived *a priori* profiles were used in the OMI NO₂ retrieval
272 process, which can sometimes cause serious smoothing errors. In order to correct such errors,
273 AKs were applied to the CMAQ model simulations in this study (Rodgers, 2000; Eskes and
274 Boersma, 2003). After the application of AKs, *a priori* information from TM4 did not
275 influence the comparison between Ω_{OMI} and $\Omega_{\text{CMAQ,AK}}$.

276

277 **3. Results and Discussions**

278 The objective of this study is to evaluate the NO_x emissions of the INTEX-B, CAPSS,
279 and REAS v1.11 inventories over East Asia by comparing two Ω obtained from the CMAQ
280 model simulations and OMI observations (Sect. 3.1). In addition, several sensitivity analyses
281 were also conducted to examine the influences of the uncertainty factors on the discrepancies
282 between $\Omega_{\text{CMAQ,AK}}$ and Ω_{OMI} (Sect. 3.2). Obviously, not all the influential factors can be
283 explored within the framework of this study. Thus, several selected issues that may be
284 important are also discussed further in Sect. 3.2.4.

285 **3.1. Comparison between CMAQ-estimated and OMI-retrieved NO₂ columns: Case 1**

286 **3.1.1. CMAQ-calculated vs. OMI-retrieved NO₂ columns**

287 In this study, the analyses were conducted for four seasons: (i) Spring (March–May,

288 2006), (ii) Summer (June–August, 2006), (iii) Fall (September–November, 2006), and (iv)
289 Winter (January–February, 2006 and December, 2006). For more detailed analyses, eight
290 focus regions were also defined: (i) Central East China (CEC), (ii) Central East China 2
291 (CEC2), (iii) South China (SC), (iv) Sichuan Basin (SB), (v) South Korea (SK), (vi) the
292 western part of Japan (JP1), (vii) the eastern part of Japan (JP2), and (viii) the entire domain
293 (DM) (refer to Fig. 2 regarding the domains).

294 Fig. 5 presents the comparison analysis between the Ω_{CMAQ} and Ω_{OMI} for the four
295 seasons over East Asia before and after the applications of the AKs. As shown in Fig. 5, the
296 CMAQ model simulations (the first and second columns) show spatially and seasonally
297 consistent patterns with OMI observations (the third column). For example, the high values of
298 the Ω_{OMI} over the densely populated and economically developed mega-city regions such as
299 Beijing, Shanghai, Hong Kong, Seoul, and Tokyo (refer to Fig. 2 regarding their locations) are
300 well captured by the CMAQ model simulations. The levels of the Ω during the winter are
301 distinctly high. Also, the low values of the Ω_{CMAQ} during the summer are well matched with
302 those from the OMI observations. The low levels of the Ω during the summer are mainly
303 caused by active NO_x chemical losses via the reaction of NO_2 with OH radicals (McConnell
304 and McElroy, 1973; Atkinson et al., 2004; Boersma et al., 2009; Han et al., 2009; Stavrou et
305 al., 2013). The uncertainties and unknown factors related to this reaction will be discussed
306 further in Sect. 3.2.4.

307 When panels (a) and (c) in Fig.5 are compared, it can be seen that the Ω_{CMAQ} is in
308 general greatly larger than the Ω_{OMI} over the regions with strong NO_x emissions. This was
309 also presented in Han et al. (2011). The large differences between the two NO_2 columns can
310 be confirmed again in panel (d) of Fig. 5. However, such a comparison *without* applying the
311 AKs is like comparing apples and oranges, and is not reasonable. Such studies have been
312 conducted over East Asia, with misleading conclusions (e.g. Ma et al., 2006; He et al., 2007;

313 Uno et al., 2007; Shi et al., 2008; Han et al., 2009; 2011). In this context, we now wish to
314 correct our previous conclusions (Han et al., 2011) here, applying the AKs to the CMAQ
315 model simulations, using the linear relationship presented in Eq. (2).

316 After the application of the AKs to the CMAQ model simulations, the comparison
317 becomes independent of *a priori* profile shape used in the NO₂ retrieval process (Eskes and
318 Boersma, 2003). In this study, when the panels (b) and (c) in Fig. 5 are compared, it can be
319 seen that the CMAQ-calculated NO₂ columns considering the AKs are much more
320 comparable to the OMI-retrieved NO₂ columns, possibly indicating that the bottom-up NO_x
321 emission used in the CMAQ model simulations would not be very greatly overestimated,
322 unlike the previous conclusion drawn by Han et al. (2011). Figs. 5(d) and 5(e) more directly
323 show the effects of the application of the AKs. When the AKs are applied, the differences are
324 greatly diminished, and are even negative, particularly over the CEC regions. The $\Omega_{\text{CMAQ,AK}}$
325 becomes smaller than the Ω_{OMI} over the CEC, SC, SK, JP1, and JP2 regions. Also, possible
326 overestimations of the bottom-up NO_x emissions were found in the CEC2 and SB regions,
327 particularly during the winter. Possible underestimations over the CEC and SC regions and
328 overestimations over the SB and CEC2 regions were also presented in the study of Lin (2012).
329 In Lin (2012), the $\Omega_{\text{GOES-CHEM,AK}}$ values were found to be about 20% and 36% lower than the
330 Ω_{OMI} over eastern China in summer and winter, respectively, whereas in the calculations
331 herein, the respective $\Omega_{\text{CMAQ,AK}}$ values were about 57% and 5% lower than the Ω_{OMI} over
332 eastern China. These differences would be caused by the constant NO_x emission fluxes and
333 relatively coarse horizontal resolutions ($0.67^\circ \times 0.5^\circ$) used in the GEOS-CHEM simulations
334 performed by Lin (2012).

335 In Table 2, we summarize the seasonal average tropospheric NO₂ columns and
336 normalized mean errors (NMEs, defined in Table A1) with and without considering the AKs
337 for the eight focus regions. It can be seen that the NMEs (with AKs applied) ranged from 40.3%

338 to 63.2% over the entire domain in Table 2. Although the differences between $\Omega_{\text{CMAQ,AK}}$ and
339 Ω_{OMI} were the smallest during the summer, as shown in Fig. 5, the NMEs showed the largest
340 values during summer. The reasons for this are discussed in detail in Sect. 3.1.2.

341 Collectively, the seasonal and regional (spatial) characteristics observed from the
342 OMI sensor were found to be captured well by the CMAQ model simulations using the
343 INTEX-B, CAPSS, and REAS emission inventories. However, some regional discrepancies
344 between the two NO_2 columns were also found, particularly during winter, indicating possible
345 underestimation of the NO_x emissions over the CEC and SC regions as well as overestimation
346 over the CEC2 and SB regions in the CMAQ model simulations. To further investigate the
347 eight regions of interest, scatter plots and statistical analyses were carried out in Sect. 3.1.2.

348 **3.1.2. Scatter plots and statistical analyses**

349 Fig. 6 presents the seasonal scatter plot analysis between the $\Omega_{\text{CMAQ,AK}}$ and Ω_{OMI} for
350 the eight focus regions defined in Fig. 2. The statistical analysis related to the scatter plots
351 was also conducted in terms of the Pearson correlation coefficient (R), linear regression slope
352 (S), and y-intercept (Y-I). As mentioned in Sect. 2.2, seasonal average of the daily Ω was
353 taken to reduce the random errors which have occurred during the NO_2 measurement and
354 retrieval processes (Fioletov et al., 2002; Monaghan et al., 2006; Johnson et al., 2007; Richter
355 et al., 2011; Clarisse et al., 2013). The use of seasonally-averaged data improved the
356 correlation coefficients from 0.49–0.63 to 0.78–0.88 over the entire domain (DM) (regarding
357 this issue, readers can compare Fig. 6 with Fig. S1). Although the correlation coefficients
358 were sometimes lower than 0.7 in Fig. 6, the two NO_2 columns correlated well, with R values
359 between 0.71 and 0.96 (also, refer to the ‘R’ values colored in Fig. 7). Slopes lower than 1.0
360 (see dashed lines in Fig. 6) were found in the “blue” regions in Fig. 5(e) such as the CEC, SC,
361 SB, JP1, and JP2 regions. These low slopes indicate the possible “underestimation” of the
362 bottom-up NO_x emissions used in the CMAQ model simulations, as discussed in Sect. 3.1.1.

363 Further statistical analyses were conducted. For absolute differences, Mean Error
364 (ME) and Mean Bias (MB) were utilized. For relative differences, Mean Normalized Gross
365 Error (MNGE), Mean Normalized Bias (MNB), Normalized Mean Error (NME), Normalized
366 Mean Bias (NMB), Mean Fractional Error (MFE), and Mean Fractional Bias (MFB) were
367 used. The Pearson correlation coefficient (R) and index of agreement (IOA) were also
368 analyzed to assess the degrees of correlations and agreement, respectively. These 10
369 performance metrics are defined and described in Table A1 (see Appendix A).

370 Fig. 7 summarizes the seasonal statistical analyses for 8 focus regions. Light colors
371 were used to indicate good agreements, while dark colors marked poor agreements. As shown,
372 the IOAs (as a measure of the degree of model prediction errors, Willmott, 1981) showed high
373 values, between 0.78 and 0.93, over the entire domain. However, the IOAs sometimes showed
374 relatively low values during the summer over several regions where large relative differences
375 were found (e.g. SB, JP1, and JP2 regions during the summer), because the IOA decreased
376 with the large difference between $\Omega_{\text{CMAQ,AK}}$ and Ω_{OMI} . As shown in Fig. 7, large MEs were
377 found over the CEC region (2.03×10^{15} to 4.51×10^{15} molecules cm^{-2}) and MBs mostly ranges
378 between -1.78×10^{15} and 1.88×10^{15} molecules cm^{-2} in East Asia, except in CEC. Again, the
379 negative values of the MBs in Fig. 7 indicate that the NO_x emissions used were possibly
380 underestimated.

381 In the seasonal perspective, all statistical parameters of the relative differences (i.e.
382 MNGE, MNB, NME, NMB, MFE, and MFB) showed large values for the summer in all the
383 regions, because the OMI-retrieved quantity in the denominator of the equations (see Table
384 A1) for the summer were relatively small versus the values of the absolute differences in the
385 numerator. In this study, the $\Omega_{\text{CMAQ,AK}}$ values over the entire domain were 7.3% and 59.7%
386 smaller than Ω_{OMI} in terms of the NMB during the summer and winter seasons, respectively.
387 In the regional perspective, the relative differences showed large values in the SC, SB, JP1,

388 and JP2 regions, where the Ω were relatively low (i.e. the same reason leading to larger
389 relative errors and biases in the summer). In this study, the $\Omega_{\text{CMAQ,AK}}$ values during winter
390 were found to be 21.8% smaller than the Ω_{OMI} over CEC, but 32.3% and 54.7% larger over
391 CEC2 and SB, respectively. Collectively, the statistical analyses showed that the $\Omega_{\text{CMAQ,AK}}$
392 were, on annual average, ~28% (from 7% to 60% with seasonal variation) smaller than the
393 Ω_{OMI} , indicating that the NO_x emissions for East Asia were possibly underestimated.

394 **3.2. Sensitivity analyses**

395 After the application of the AKs, both the $\Omega_{\text{CMAQ,AK}}$ and Ω_{OMI} became much more
396 comparable with each other as shown in Fig. 5. Even so, this comparison study still has
397 several uncertainties. Because of the uncertainties, it is difficult to directly relate the
398 differences between the $\Omega_{\text{CMAQ,AK}}$ and Ω_{OMI} to under- or over-estimations in the NO_x
399 emissions. Therefore, examination of the uncertainty issues was carried out herein. The issues
400 selected for examination in this study were as follows: (i) the monthly variation in NO_x
401 emissions; (ii) influences of the different magnitude of NO_x emissions; and (iii) different
402 parameterizations of the reaction probability of N_2O_5 onto aerosols in the CMAQ model
403 simulations. These three issues were selected for the following reasons: (i) the emission flux
404 in East Asia is believed to be one of the most uncertain factors, and its magnitude can vary
405 greatly depending on monthly variation as well as methodology and activity data used to
406 estimate the emission fluxes (Cases 2 and 3) (Wang et al., 2007; Zhang et al., 2007; Han et al.,
407 2009; Klimont et al., 2009; Zhang et al., 2009; Xing et al., 2011); and (ii) although the
408 condensation of N_2O_5 radicals is a major NO_x loss processes during the winter and thus may
409 significantly influence the tropospheric NO_2 columns, the magnitudes of $\gamma_{\text{N}_2\text{O}_5}$ remain highly
410 uncertain, ranging between 0.1 and 0.001 (Case 4) (Dentener and Crutzen, 1993; Jacob, 2000;
411 Brown et al., 2006; Davis et al., 2008; Macintyre and Evans, 2010). Sect. 3.2 is therefore
412 devoted to these issues, which are addressed with sensitivity analyses.

413 3.2.1. Monthly variation in NO_x emissions: Case 2

414 First, the monthly variations of NO_x emissions over China were investigated,
415 choosing different monthly variations from the base-case emission. In this sensitivity run (see
416 Table 1), we applied a more drastic/extreme monthly variation of the NO_x emissions (thick-
417 black line in Fig. 1) (Han et al., 2009) to the CMAQ model simulation over China in this one-
418 year run. The main reason we did this is that, as shown in Figs. 5 and 6, the $\Omega_{\text{CMAQ,AK}}$ was
419 smaller than the Ω_{OMI} , over several main regions (such as CEC and main mega-city areas like
420 Hong Kong and Shanghai) in China, particularly during the “cold months”. It should be noted
421 that during the cold months, the NO_x emission fluxes reported in Han et al. (2009) for China
422 were 1.20 times larger than those from the INTEX-B inventory.

423 The results are presented in Fig. 8. The spatial distributions of the $\Omega_{\text{CMAQ,AK}}$ and Ω_{OMI}
424 are shown in Fig. 8 for the four seasons. As indicated in Table S1 in the supplementary
425 materials, the application of the AKs again greatly reduced the errors and biases between the
426 two tropospheric NO₂ columns in this sensitivity test. As expected, the $\Omega_{\text{CMAQ,AK}}$ in Fig. 8 (a)
427 generally increased for the spring and winter, whereas it decreased for the summer and fall,
428 compared with the values in Fig. 5 (b). These increases in the $\Omega_{\text{CMAQ,AK}}$ for the winter
429 produced better agreement with the Ω_{OMI} , particularly over the CEC region, showing that the
430 MBs over CEC during the winter decreased from -3.10×10^{15} molecule cm⁻² to -7.42×10^{14}
431 molecule cm⁻² (see the average NO₂ columns and NMEs in Tables 2 and S1). However, as
432 shown in Tables 2 and S1, the situations became worse, except for the CEC region, showing
433 significant increases in NMEs, compared with the NMEs in cases using the monthly variation
434 of the INTEX-B inventory taken from Zhang et al. (2009). Even larger (more serious)
435 differences between the two NO₂ columns in Fig. 8 (c) were found over other regions of
436 China (CEC2, SC, and SB) than those shown in Fig. 5 (e) in terms of errors and biases. For
437 example, the MBs during the winter increased from 2.74×10^{15} , -2.92×10^{13} , and 1.88×10^{15}

438 molecule cm^{-2} to 5.26×10^{15} , 7.10×10^{15} , and 5.35×10^{15} molecule cm^{-2} over CEC2, SC, and SB,
439 respectively.

440 Further detailed analyses over the eight focus regions were carried out, and the scatter
441 plots and statistical analyses are presented in Figs. S2 and S3 of the supplementary materials.
442 Collectively, the sensitivity test showed that the monthly variations of the OMI observations
443 were better captured by the CMAQ model simulations using the monthly variations of the
444 INTEX-B inventory than those from Han et al. (2009), although the monthly variations in the
445 NO_x emission of the INTEX-B inventory still remain uncertain in China, particularly over the
446 CEC region.

447 **3.2.2. Another NO_x emission inventory (REAS v1.11): Case 3**

448 There is another NO_x emission inventory available in China: the REAS v1.11
449 emission inventory for 2006 (Ohara et al., 2007). Thus, in this section, the REAS emission
450 inventory, a frequently used bottom-up inventory established by the National Institute of
451 Environmental Studies (NIES) in Japan, was tested over China for January (a cold month) in
452 order to determine the influence of different NO_x emissions on the tropospheric NO_2 columns.
453 Because the REAS v1.11 inventory does not include monthly variation, the same monthly
454 variation of the INTEX-B inventory was also applied to this sensitivity study. The NO_x
455 emissions between the INTEX-B and REAS inventories differed greatly over China. For
456 example, the annual NO_x emissions from the INTEX-B inventory were 2.48, 2.22, 1.60, and
457 $0.57 \text{ Tg N yr}^{-1}$ over the CEC, CEC2, SC, and SB regions, respectively, whereas those from the
458 REAS inventory were 1.93, 1.56, 1.40, and $0.40 \text{ Tg N yr}^{-1}$, respectively, over the same regions.

459 The results are presented in Fig. 9 and Table S2. The application of the AKs to the
460 CMAQ model simulations were also taken into account in this comparison (see Table S2). As
461 expected, the $\Omega_{\text{CMAQ,AK}}$ decreased significantly over China, when the REAS NO_x emissions
462 were used (refer to Table S2 in the supplementary materials). Although the absolute

463 differences between the $\Omega_{\text{CMAQ,AK}}$ and Ω_{OMI} became smaller over the CEC2 and SB regions,
464 much large underestimates were found over the CEC region, compared with the case of the
465 INTEX-B inventory as shown in Fig. 9.

466 Collectively, our results indicate that (i) the NO_x emission fluxes from the REAS
467 inventory are also underestimated over China (particularly, over the CEC region), (ii) both
468 NO_x emission inventories (INTEX-B and REAS) showed underestimation over the CEC
469 region and the Hong Kong area, and (iii) accurate spatial distributions of NO_x emissions and
470 the magnitude of NO_x emissions were important factors to reduce the degree of disagreement
471 between the CTM-estimated and satellite-retrieved NO_2 columns. For better agreement
472 between the $\Omega_{\text{CMAQ,AK}}$ and Ω_{OMI} over China, a combination of the two emission inventories
473 may be a good practical attempt in the CMAQ model simulations over East Asia, based on
474 this result. That is, the INTEX-B NO_x emissions data tended to produce better results over the
475 CEC region, whereas the REAS NO_x emissions data tended to generate better results over the
476 CEC2 and SB regions. However, this issue (i.e., the combination of the two emission
477 inventories) needs to be examined using a more sophisticated approach, and should be
478 investigated further.

479

480 **3.2.3. Reaction probability of N_2O_5 : Case 4**

481 We explored the issue of reaction probability of N_2O_5 ($\gamma_{\text{N}_2\text{O}_5}$) onto aerosols, because a
482 relatively large discrepancy between the $\Omega_{\text{CMAQ,AK}}$ and Ω_{OMI} was found, particularly during
483 the winter season. During the winter season, the condensation of N_2O_5 into atmospheric
484 particles is an important NO_x loss process (Dentener and Crutzen, 1993; Brown et al., 2004;
485 2006). Thus, it can affect the CMAQ-simulated NO_2 columns ($\Omega_{\text{CMAQ,AK}}$). Although it is an
486 important physico-chemical NO_x loss process during the winter, the magnitude of $\gamma_{\text{N}_2\text{O}_5}$ has
487 been a controversial issue. In this study, five $\Omega_{\text{CMAQ,AK}}$ from the CMAQ model simulations

488 with five different $\gamma_{\text{N}_2\text{O}_5}$ parameterizations were compared with the Ω_{OMI} over East Asia.
489 These five parameterizations are from the works of: (i) Dentener and Crutzen (1993), (ii)
490 Riemer et al. (2003), (iii) a combination of Riemer et al. (2003) and Evans and Jacob (2005),
491 (iv) Davis et al. (2008), and (v) Brown et al., (2006). The mathematical expressions for these
492 parameterizations are summarized briefly in Table 3. In the Dentener and Crutzen's
493 parameterization (1993), they used a fixed value of $\gamma_{\text{N}_2\text{O}_5}$ of 0.1 in their global CTM
494 simulation (Scheme I in Table 3). In Riemer et al.'s parameterization (2003), $\gamma_{\text{N}_2\text{O}_5}$ is a main
495 function of the acidity of the particles (Scheme II). In the combined parameterization of Evans
496 and Jacob (2006) and Riemer et al. (2003), $\gamma_{\text{N}_2\text{O}_5}$ is a function of relative humidity (RH),
497 temperature, and the acidity of the particles (Scheme III, standard scheme). In Davis et al.
498 (2008)'s parameterization, $\gamma_{\text{N}_2\text{O}_5}$ is a function of all the factors, such as RH, temperature, the
499 acidity of the particles, and the mixing state (Scheme IV). Finally, for Brown et al. (2006)'s
500 parameterization, we used a fixed minimum value of $\gamma_{\text{N}_2\text{O}_5}$ of 10^{-3} in the CMAQ model
501 simulation (Scheme V).

502 The comparison results are presented in Fig. 10. As shown in Fig. 10 and Table 4, the
503 $\Omega_{\text{CMAQ,AK}}$ with the Brown et al. (2006) parameterization were ~19% larger than those with the
504 standard Scheme (III) over East Asia. This indicates that Brown et al.'s parameterization
505 resulted in the smallest NO_x loss rates (or nitrate formation rates) via this physico-chemical
506 reaction pathway.

507 In contrast, the application of the Dentener and Crutzen's parameterization to the
508 CMAQ model simulation produced the smallest $\Omega_{\text{CMAQ,AK}}$ in East Asia, indicating the fastest
509 NO_x loss rates, due to the large $\gamma_{\text{N}_2\text{O}_5}$. These results suggest that Brown et al.'s $\gamma_{\text{N}_2\text{O}_5}$ (= 0.001)
510 may be smaller than the real value, while Dentener and Crutzen's $\gamma_{\text{N}_2\text{O}_5}$ (= 0.1) is probably
511 larger. Other than Brown et al.'s and Dentener and Crutzen's parameterizations, it was found
512 that there was almost no significant or practical difference in the $\Omega_{\text{CMAQ,AK}}$ among the other

513 three Schemes, II, III, and IV (also, refer to Table 4).

514 As shown in Fig. 10 and Table 4, Schemes II, III, and IV tended to produce better
515 $\Omega_{\text{CMAQ,AK}}$ data over East Asia than Schemes I and V, compared with Ω_{OMI} . More recently,
516 Brown et al. (2009) and Bertram et al. (2009) also discussed that the $\gamma_{\text{N}_2\text{O}_5}$ values being used
517 currently in regional/global CTMs were generally larger than those from their observed $\gamma_{\text{N}_2\text{O}_5}$.
518 In addition to the issue of $\gamma_{\text{N}_2\text{O}_5}$, it should be noted that the aerosol surface density (A) is
519 another uncertain factor that can influence the $\Omega_{\text{CMAQ,AK}}$, because the rate constant ($k_{\text{N}_2\text{O}_5}$) of
520 the physico-chemical reaction also depends on the aerosol surface density (refer to the
521 Schwartz formula, $k_{\text{N}_2\text{O}_5} = \frac{A \cdot C_{\text{mean}} \gamma_{\text{N}_2\text{O}_5}}{4}$). Although all of these issues are arguable, our
522 results show that the $\gamma_{\text{N}_2\text{O}_5}$ parameterizations can certainly influence the levels of Ω_{NO_2} in East
523 Asia, particularly during the winter season.

524 **3.2.4. More uncertainties and outlooks**

525 As mentioned previously, in this type of analysis all types of temporal variation are
526 potentially important and should therefore be taken into account. A sensitivity analysis on the
527 monthly variation in the NO_x emissions in China was performed in Sect. 3.2.1, showing that
528 the monthly variations in NO_x emissions were an important factor. In contrast, there is only
529 limited information on other temporal variation, such as daily and weekly variation in NO_x
530 emissions in East Asia. Unfortunately, no emission inventory in East Asia can provide us with
531 this level of information. Regarding the issue of the temporal variation, the future Korean
532 Geostationary Environmental Monitoring Spectrometer (GEMS) sensor, which is planned to
533 be launched in 2018, will be able to help to obtain such information on daily and weekly
534 variation in the NO_x emissions over East Asia (Kim, 2012).

535 There is also some level of uncertainty in the NO_2 -to- NO ratios, as discussed
536 previously by Richter et al. (2005) and Han et al. (2009). This factor may be important,

537 because every satellite remote-sensor monitors only NO₂ columns, not NO_x columns. The
 538 NO₂-to-NO ratios are affected seriously by anthropogenic and biogenic VOC (AVOC and
 539 BVOC) emissions and their mixing ratios. For example, if we assume a photo-stationary state,
 540 the NO₂-to-NO ratios can be influenced by the mixing ratios of ozone and HO₂, CH₃O₂, and
 541 RO₂ radicals, as shown in the following formula:

$$542 \quad \frac{[NO_2]}{[NO]} = \frac{k_1[O_3] + k_2[HO_2] + k_3[CH_3O_2] + k_4[RO_2]}{J_1} \quad (3)$$

543 where J_1 is the NO₂ photolysis rate constant (s⁻¹) and k_1 (=1.81×10⁻¹⁴ at 298 K), k_2 (=8.41×10⁻¹²
 544 at 298 K), k_3 (=7.29×10⁻¹² at 298 K), and k_4 (=9.04×10⁻¹² – 2.80×10⁻¹¹ at 298 K) are the
 545 reaction rate constants (cm³ molecules⁻¹ s⁻¹) for NO+O₃, NO+HO₂, NO+CH₃O₂, and NO+RO₂
 546 reactions, respectively. Although k_1 is the smallest among the 4 reaction rate constants, the
 547 NO₂ to-NO ratio tends to be determined by the NO+O₃ reaction, together with the photolysis
 548 of NO₂ (J_1), because ambient O₃ mixing ratios usually occur in several tens of ppb. However,
 549 the NO+HO₂ and NO+RO₂ reactions during summer have almost equivalent (non-negligible)
 550 contribution to the NO₂-to-NO ratios, for example, over the SC region where BVOC
 551 emissions are active. In addition, the mixing ratios of ozone, HO₂, CH₃O₂, and RO₂ in Eq. (3)
 552 can be affected by AVOC and BVOC emissions and their mixing ratios, which are believed to
 553 be highly uncertain in East Asia (Fu et al., 2007; Lin et al., 2012; Han et al., 2013).

554 Third, as also discussed by Han et al. (2009), there is large uncertainty in the NO_x
 555 loss rates (or NO_x lifetime) in global/regional CTMs. Many groups have reported that the
 556 uncertainty in the NO_x loss rate is related to several factors (Lin et al., 2012; Stavrakou et al.,
 557 2013), such as nitric acid formation via the NO₂+OH reaction (Atkinson et al., 2004; Mollner
 558 et al., 2010; Sander et al., 2011; Henderson et al., 2012) and NO+HO₂ reaction (Butkovskaya
 559 et al., 2005; 2009), isoprene chemistry (e.g. OH regeneration) during the summer months
 560 (Butler et al., 2008; Lelieveld et al., 2008; Archibald et al., 2010; Kubistin et al., 2010; Pugh

561 et al., 2010), alkyl nitrate formation (Browne and Cohen, 2012; Browne et al., 2013),
562 “daytime” HONO chemistry (Harris et al., 1982; Svennson et al., 1987; Rondon and
563 Sanhueza, 1989; Pagsberg et al., 1997; Stemmler et al., 2006; Sörgel et al., 2011; Zhou et al.,
564 2011), inclusion of in-plume photochemistry (Karamchandani et al., 2000; Song et al., 2003;
565 Kim et al., 2009; Song et al., 2010), and peroxyacetyl nitrate (PAN) formation (Robert et al.,
566 2002).

567 Recently, modeling uncertainties including meteorological parameters were discussed
568 comprehensively by Lin et al. (2012). They reported that when tropospheric NO₂ columns
569 from several sensitivity simulations were compared with those from standard simulations, the
570 largest impact on the tropospheric NO₂ columns was caused by modifying the reaction
571 probability of HO₂ onto aerosols (i.e. γ_{HO_2}), followed by the modifications of cloud optical
572 depth, HNO₃ formation rate via NO₂+OH, $\gamma_{\text{N}_2\text{O}_5}$, and aromatic species emissions. It was also
573 reported in their study that modification of all the parameters could increase the tropospheric
574 NO₂ columns by 18% during July and by 8% during January. Although the results herein can
575 be complementary to those reported by Lin et al. (2012), all of these issues are on-going and
576 open questions.

577 In addition to the issues mentioned above, in the CTM simulations there are
578 additional uncertainties in biological NO_x emissions from soil and pyrogenic NO_x emissions
579 (e.g., biomass burning NO_x emissions) (Bertram et al., 2005; Jaeglé et al., 2005; Hudman et
580 al., 2010; Lin, 2012). However, for example, the biological NO_x emissions from soil are
581 usually more active during the summer. During the summer, the NO_x loss rates are so fast that
582 considerations of additional NO_x emissions would hardly change the CTM-calculated NO₂
583 columns (Boersma et al., 2009; Han et al., 2009). The same is true for the issues of OH
584 recycling and isoprene-derived alkyl nitrate formation mentioned above. There are
585 uncertainties and unknown chemistry related to isoprene, but, due to the fast NO_x loss rates

586 during the summer, it has been found that these factors do not greatly affect the $\Omega_{\text{CMAQ,AK}}$
587 during the summer in our test runs (data not shown).

588 On the other hand, in the view of satellite observations, there are errors and
589 uncertainties in the retrievals of the NO_2 vertical columns and the AKs. There are also several
590 NO_2 vertical column products from different sensors (e.g. GOME, OMI, SCIAMACHY, and
591 GOME-2) and from different algorithms (e.g. KNMI, Bremen, BIRA, Harvard Smithsonian,
592 and NASA). For example, the different NO_2 products sometimes show considerable
593 differences (Herron-Thorpe et al., 2010). Overall, different combinations of these sensors and
594 algorithms can produce different NO_2 column products. Thus, in this type of comparison
595 analysis, all the uncertainty factors mentioned above should be taken into account cautiously.

596

597 **4. Summary and conclusions**

598 The accuracy of bottom-up NO_x emission fluxes from the INTEX-B, CAPSS, and
599 REAS emission inventories were investigated through comparisons between the $\Omega_{\text{CMAQ,AK}}$
600 and Ω_{OMI} in East Asia. For the comparison study, the CMAQ model simulations were carried
601 out over 12 months in 2006 over East Asia. Also, for the direct comparison between the
602 Ω_{CMAQ} and Ω_{OMI} , we applied the AKs to the CMAQ model simulations. This study showed
603 that the seasonal and regional/spatial characteristics from the OMI observations were captured
604 well by the CMAQ model simulations using the INTEX-B, CAPSS, and REAS v1.11
605 emission inventories over East Asia. It was also found that the normalized mean errors
606 (NMEs) between the $\Omega_{\text{CMAQ,AK}}$ and Ω_{OMI} for the data from East Asia decreased, from ~80% to
607 ~46%, from ~79% to ~44%, and from ~98% to ~40% during the spring, fall, and winter,
608 respectively, compared with the NME between the Ω_{CMAQ} and Ω_{OMI} (without AKs
609 application). Overall, the $\Omega_{\text{CMAQ,AK}}$ were an annual average of ~28% (in terms of the NMB;
610 from 7% to 60% with seasonal variation) smaller in East Asia than the Ω_{OMI} , indicating

611 possible underestimations of the NO_x emissions used in this study.

612 To assess the seasonal and spatial discrepancies, several sensitivity studies, shown in
613 Table 1, were performed considering several uncertainty factors such as (i) monthly variation
614 of NO_x emission, (ii) influences of different NO_x emissions in East Asia, and (iii) reaction
615 probabilities of N₂O₅. In Table 5, we summarize the relative changes in the NO₂ columns
616 from the sensitivity simulations with respect to those from the standard simulation (Case 1).
617 From the sensitivity simulations, we found that:

- 618 – Monthly variations in NO_x emissions have a strong impact on tropospheric NO₂
619 columns. The relative changes ranged from -31.16% to 65.37% over China, when the
620 monthly factors from Han et al. (2009) were used. However, Han et al.'s monthly
621 variations (2009) resulted in even larger discrepancies between $\Omega_{\text{CMAQ,AK}}$ and Ω_{OMI}
622 over several regions in China. The monthly variations of the INTEX-B NO_x inventory
623 had a tendency to result in better agreements between the $\Omega_{\text{CMAQ,AK}}$ and Ω_{OMI} over
624 China.
- 625 – As shown in Table 5, when REAS v1.11 inventory data over China were used in the
626 CMAQ model simulations, the $\Omega_{\text{CMAQ,AK}}$ become -31.45% to -58.44% lower over
627 China than those from the case with the INTEX-B inventory. Based on this, the NO_x
628 emissions from the REAS v1.11NO_x emissions appeared to be more underestimated
629 over China than the INTEX-B NO_x emissions.
- 630 – In the sensitivity test of γ_{N2O5} , it appeared that the γ_{N2O5} parameterization would not
631 be a negligible factor, particularly during the winter. The $\Omega_{\text{CMAQ,AK}}$ from Brown et al.
632 (2006)'s parameterization were ~19% larger over East Asia than the $\Omega_{\text{CMAQ,AK}}$ from
633 the combined parameterization of Riemer et al. (2003) and Evans and Jacob (2006).
634 In this study, the conventional γ_{N2O5} parameterizations (Schemes II, III, and IV)

635 showed almost no practical differences in the $\Omega_{\text{CMAQ,AK}}$ and tended to produce better
636 $\Omega_{\text{CMAQ,AK}}$ data over East Asia than Schemes I and V.

637

638 One of the main driving forces of this study was to correct our previous conclusions
639 (Han et al., 2011), in which AKs were not employed for the comparison between the Ω_{OMI} and
640 Ω_{CMAQ} . Again, this study indicated that the bottom-up NO_x emissions of the INTEX-B,
641 CAPSS, and REAS v1.11 inventories used in the CMAQ model simulations would be rather
642 underestimated over East Asia. In the sensitivity studies, the influences of different NO_x
643 emissions and monthly variation in NO_x emissions can also significantly influence the levels
644 of the $\Omega_{\text{CMAQ,AK}}$ in East Asia. Moreover, we showed that the $\gamma_{\text{N}_2\text{O}_5}$ parameterization could be
645 another important factor in the winter. Because other possible uncertainty factors still exist, as
646 discussed in Sect. 3.2.4, further analyses are definitely necessary in future studies.

647 The estimation of “top-down” NO_x emissions has also been carried out in East Asia
648 (Stavrakou et al., 2008; Lin et al., 2010; Mijling et al., 2013) using satellite-derived NO_2
649 columns. However, in such top-down estimations, other uncertain (limiting) factors exist,
650 such as the lifetime of NO_x (i.e., τ_{NO_x}). The uncertainty in τ_{NO_x} is also linked with the factors
651 discussed herein in Sect. 3.2.4. In addition, even in the top-down NO_x emission, the random
652 and smoothing errors should be reduced/minimized via temporal and/or spatial averaging and
653 the application of AKs, respectively, as demonstrated herein.

654 Improvements in the NO_x emissions data or evaluation of the accuracy of bottom-up
655 NO_x emission fluxes in East Asia can improve air quality modeling and chemical weather
656 forecasting over East Asia. Thus, much effort should be focused on this issue in the future,
657 particularly on the circumstances over East Asia. In this context, efforts in inverse modeling
658 to improve the NO_x emissions data over East Asia, such as adjoint modeling with measured
659 data and top-down estimations of the NO_x emissions with satellite observations, could also

660 contribute to improving the performance of air quality modeling and the accuracy of chemical
661 weather forecasting over East Asia (Park et al., 2013).

662

663 **Acknowledgements**

664 This research was supported by the GEMS program of the Ministry of Environment, Korea,
665 as part of the Eco Innovation Program of KEITI (2012000160004). This work was also
666 supported by the Basic Science Research Program through the National Research Foundation
667 of Korea (NRF), funded by the Ministry of Science, ICT & Future Planning
668 (2014R1A1A1004523), and by the Korea Meteorological Administration Research and
669 Development Program under Grant CATER 2012-7110. We would like to acknowledge the
670 use of the tropospheric NO₂ column data from www.temis.nl.

671

672

673 **Appendix A**

674 For statistical analyses between the CMAQ-calculated and OMI-retrieved tropospheric NO₂
 675 columns, several statistical parameters below are introduced in Table A1.

- 676 1. Absolute errors and biases: The Mean Error (ME) and Mean Bias (MB) are statistical
 677 parameters used to measure how close the estimated values ($\Omega_{CMAQ,AK}$ in this study) are to
 678 the observed values (Ω_{OMI} in this study). The distinction between the two parameters is that
 679 the MB provides information on overestimation (i.e. positive values) or underestimation
 680 (i.e. negative values) of the estimated values.
- 681 2. Relative errors and biases: The Mean Normalized Gross Error (MNGE) and Mean
 682 Normalized Bias (MNB) are statistical parameters used to measure the relative differences
 683 normalized by the observed values. The values of the MNGE and MNB can be
 684 significantly inflated (or overstated), when observations are sometimes close to zero. In
 685 this case, the Normalized Mean Error (NME) and Normalized Mean Bias (NMB) can be
 686 useful statistical parameters, because they avoid over-inflating the measured range.
 687 However, these bias parameters have an issue of asymmetry, meaning that overestimations
 688 (i.e., $+\infty$) are weighted more than the equivalent underestimations (i.e., -100), as shown in
 689 Table A1. The Mean Fractional Bias (MFB) provides equal weight to both sides, which
 690 range from -200 to +200, as shown in Table A1.
- 691 3. Agreements: The Pearson correlation coefficient (R) is a statistical parameter to measure
 692 the degree to which both the estimated and observed values are linearly related. The value
 693 of R=1 indicates perfect agreement between both values, whereas R=0 means no linear
 694 relationship. The Pearson correlation coefficient can sometimes be numerically unstable,
 695 depending on the sample size. The Index of Agreement (IOA) is a standardized measure of
 696 the degree of estimation error, ranging from 0 to 1 (Willmott, 1981). Unlike the Pearson
 697 correlation coefficient, the IOA can account for additive and proportional differences in the
 698 estimated and observed means and variances. The value of 0 indicates no agreement
 699 between the estimated and observed values, whereas the value of 1 indicates perfect
 700 agreement.

701
 702 **Table A1. Statistical parameters used in this study.**

Parameters (unit)	Equations ¹⁾	Range
Mean Error (molecules cm ⁻²)	$ME = \frac{1}{N} \sum_{i=1}^N \Omega_{CMAQ,AK} - \Omega_{OMI} $	0 to $+\infty$
Mean Bias (molecules cm ⁻²)	$MB = \frac{1}{N} \sum_{i=1}^N (\Omega_{CMAQ,AK} - \Omega_{OMI}) = \overline{\Omega_{CMAQ,AK}} - \overline{\Omega_{OMI}}$	$-\overline{\Omega_{NO2/OMI}}$ to $+\infty$
Mean Normalized Gross Error (%)	$MNGE = \frac{1}{N} \sum_{i=1}^N \frac{ \Omega_{CMAQ,AK} - \Omega_{OMI} }{\Omega_{OMI}} \times 100$	0 to $+\infty$
Mean Normalized Bias (%)	$MNB = \frac{1}{N} \sum_{i=1}^N \left(\frac{\Omega_{CMAQ,AK} - \Omega_{OMI}}{\Omega_{OMI}} \right) \times 100$	-100 to $+\infty$
Normalized Mean Error (%)	$NME = \frac{\sum_{i=1}^N \Omega_{CMAQ,AK} - \Omega_{OMI} }{\sum_{i=1}^N \Omega_{OMI}} \times 100$	0 to $+\infty$
Normalized Mean Bias (%)	$NMB = \frac{\sum_{i=1}^N (\Omega_{CMAQ,AK} - \Omega_{OMI})}{\sum_{i=1}^N \Omega_{OMI}} \times 100$	-100 to $+\infty$

Mean Fractional Error (%)	$MFE = \frac{1}{N} \sum_{i=1}^N \left(\frac{ \Omega_{CMAQ,AK} - \Omega_{OMI} }{\frac{\Omega_{CMAQ,AK} + \Omega_{OMI}}{2}} \right) \times 100$	0 to +200
Mean Fractional Bias (%)	$MFB = \frac{1}{N} \sum_{i=1}^N \left(\frac{\Omega_{CMAQ,AK} - \Omega_{OMI}}{\frac{\Omega_{CMAQ,AK} + \Omega_{OMI}}{2}} \right) \times 100$	-200 to +200
Pearson correlation coefficient (dimensionless)	$R = \frac{\sum_{i=1}^N (\Omega_{CMAQ,AK} - \overline{\Omega_{CMAQ,AK}})(\Omega_{OMI} - \overline{\Omega_{OMI}})}{\sqrt{\sum_{i=1}^N (\Omega_{CMAQ,AK} - \overline{\Omega_{CMAQ,AK}})^2 \sum_{i=1}^N (\Omega_{OMI} - \overline{\Omega_{OMI}})^2}}$	-1 to +1
Index of agreement (dimensionless)	$IOA = 1 - \frac{\sum_{i=1}^N (\Omega_{CMAQ,AK} - \Omega_{OMI})^2}{\sum_{i=1}^N (\Omega_{CMAQ,AK} - \overline{\Omega_{OMI}} + \Omega_{OMI} - \overline{\Omega_{OMI}})^2}$	0 to +1

703 ¹⁾ $\Omega_{CMAQ,AK}$ and Ω_{OMI} indicate the CMAQ-calculated NO₂ columns with the consideration of AKs and the OMI-
704 retrieved NO₂ columns, respectively. N represents the number of data samples.

References

- 705
706
707 Archibald, A. T., Cooke, M. C., Utembe, S. R., Shallcross, D. E., Derwent, R. G., and
708 Jenkin, M. E.: Impacts of mechanistic changes on HO_x formation and recycling in the
709 oxidation of isoprene, *Atmos. Chem. Phys.*, 10, 8097-8118, doi:10.5194/acp-10-8097-
710 2010, 2010.
- 711 Atkinson, R., Baulch, D. L., Cox, R. A., Crowley, J. N., Hampson, R. F., Hynes, R. G.,
712 Jenkin, M. E., Rossi, M. J., and Troe, J.: Evaluated kinetic and photochemical data for
713 atmospheric chemistry: Volume I - gas phase reactions of O_x, HO_x, NO_x and
714 SO_x species, *Atmos. Chem. Phys.*, 4, 1461-1738, doi:10.5194/acp-4-1461-2004, 2004.
- 715 Bertram, T. H., Heckel, A., Richter, A., Burrows, J. P., and Cohen, R. C.: Satellite
716 measurements of daily variations in soil NO_x emissions, *Geophys. Res. Lett.*, 32(24),
717 L24812, doi:10.1029/2005GL024640, 2005.
- 718 Bertram, T. H., Thornton, J. A., Riedel, T. P., Middlebrook, A. M., Bahreini, R., Bates, T. S.,
719 Quinn, P. K., and Coffman, D. J.: Direct observations of N₂O₅ reactivity on ambient
720 aerosol particles, *Geophys. Res. Lett.*, 36, L19803, doi:10.1029/2009GL040248, 2009.
- 721 Binkowski, F. S. and Roselle, S. J.: Models-3 Community Multi-scale Air Quality (CMAQ)
722 model aerosol components: 1. model description, *J. Geophys. Res.*, 108 (D6), 4183,
723 doi:10.1029/2001JD001409, 2003.
- 724 Boersma, K. F., Eskes, H. J., Veefkind, J. P., Brinksma, E. J., van der A, R. J., Sneep, M.,
725 van den Oord, G. H. J., Levelt, P. F., Stammes, P., Gleason, J. F., and Bucsela, E. J.:
726 Near-real time retrieval of tropospheric NO₂ from OMI, *Atmos. Chem. Phys.*, 7, 2103-
727 2118, doi:10.5194/acp-7-2103-2007, 2007.
- 728 Boersma, K. F., Jacob, D. J., Trainic, M., Rudich, Y., DeSmedt, I., Dirksen, R., and
729 Eskes, H. J.: Validation of urban NO₂ concentrations and their diurnal and seasonal
730 variations observed from the SCIAMACHY and OMI sensors using in situ surface
731 measurements in Israeli cities, *Atmos. Chem. Phys.*, 9, 3867-3879, doi:10.5194/acp-9-
732 3867-2009, 2009.
- 733 Boersma, K. F., Eskes, H. J., Dirksen, R. J., van der A, R. J., Veefkind, J. P., Stammes, P.,
734 Huijnen, V., Kleipool, Q. L., Sneep, M., Claas, J., Leitão, J., Richter, A., Zhou, Y., and
735 Brunner, D.: An improved tropospheric NO₂ column retrieval algorithm for the Ozone
736 Monitoring Instrument, *Atmos. Meas. Tech.*, 4, 1905-1928, doi:10.5194/amt-4-1905-
737 2011, 2011a.
- 738 Boersma, K. F., Braak, R., and van der A, R. J.: Dutch OMI NO₂ (DOMINO) data product
739 v2.0 HE5 data file user manual, TEMIS website, available
740 at:<http://www.temis.nl/airpollution/no2.html> (last access: 2 Oct 2014) 2011b.
- 741 Brown, S. S., Dibb, J. E., Stark, H., Aldener, M., Vozella, M., Whitlow, S., Williams, E. J.,
742 Lerner, B. M., Jakoubek, R., Middlebrook, A. M., DeGouw, J. A., Warneke, C., Goldan,
743 P. D., Kuster, W. C., Angevine, W. M., Sueper, D. T., Quinn P. K., Bates, T. S.,
744 Meagher, J. F., Fehsenfeld, F. C., and Ravishankara, A. R.: Nighttime removal of NO_x
745 in the summer marine boundary layer, *Geophys. Res. Lett.*, 31, L07108, doi:
746 10.1029/2004GL019412, 2004.
- 747 Brown, S. S., Ryerson, T. B., Wollny, A. G., Brock, C. A., Peltier, R., Sullivan, A. P., Weber,
748 R. J., Dube, W. P., Trainer, M., Meagher, J. F., Fehsenfeld, F. C., and Ravishankara, A.
749 R.: Variability in nocturnal nitrogen oxide processing and its role in regional air
750 quality, *Science*, 311, 67-70, 2006.
- 751 Brown, S. S., Dubé, W. P., Fuchs, H., Ryerson, T. B., Wollny, A. G., Brock, C. A., Bahreini, R.,
752 Middlebrook, A. M., Neuman, J. A., Atlas, E., Roberts, J. M., Osthoff, H. D., Trainer,
753 M., Fehsenfeld, F. C., and Ravishankara, A. R.: Reactive Uptake Coefficients for N₂O₅

754 Determined from Aircraft Measurements during the Second Texas Air Quality Study:
755 Comparison to Current Model Parameterizations, *J. Geophys. Res.* 114:D00F10.
756 doi:10.1029/2008JD011679, 2009.

757 Browne, E. C. and Cohen, R. C.: Effects of biogenic nitrate chemistry on the NO_x lifetime in
758 remote continental regions, *Atmos. Chem. Phys.*, 12, 11917-11932, doi:10.5194/acp-
759 12-11917-2012, 2012.

760 Browne, E. C., Min, K.-E., Wooldridge, P. J., Apel, E., Blake, D. R., Brune, W. H.,
761 Cantrell, C. A., Cubison, M. J., Diskin, G. S., Jimenez, J. L., Weinheimer, A. J.,
762 Wennberg, P. O., Wisthaler, A., and Cohen, R. C.: Observations of total RONO₂ over
763 the boreal forest: NO_x sinks and HNO₃ sources, *Atmos. Chem. Phys.*, 13, 4543-4562,
764 doi:10.5194/acp-13-4543-2013, 2013.

765 Butkovskaya, N. I., Kukui, A., Pouvesle, N., and Le Bras, G.: Formation of Nitric Acid in the
766 Gas-Phase HO₂ + NO Reaction: Effects of Temperature and Water Vapor, *J. Phys.*
767 *Chem. A*, 109(29), 6509–6520, doi:10.1021/jp051534v, 2005.

768 Butkovskaya, N., Rayez, M.-T., Rayez, J.-C., Kukui, A., and Le Bras, G.: Water vapor effect
769 on the HNO₃ yield in the HO₂ + NO reaction: Experimental and theoretical evidence, *J.*
770 *Phys. Chem. A*, 113(42), 11327–11342, doi: 10.1021/jp811428p, 2009.

771 Butler, T. M., Taraborrelli, D., Brühl, C., Fischer, H., Harder, H., Martinez, M., Williams, J.,
772 Lawrence, M. G., and Lelieveld, J.: Improved simulation of isoprene oxidation
773 chemistry with the ECHAM5/MESSy chemistry-climate model: lessons from the
774 GABRIEL airborne field campaign, *Atmos. Chem. Phys.*, 8, 4529-4546,
775 doi:10.5194/acp-8-4529-2008, 2008.

776 Byun, D. W. and Schere, K. L.: Review of the governing equations, computational algorithm,
777 and other components of the Models-3 Community Multi-scale Air Quality (CMAQ)
778 Modeling system, *Appl. Mech. Rev.*, 59(2), 51–77, 2006.

779 Carter, W. P. L.: Implementation of the SAPRC-99 Chemical Mechanism into the Models-3
780 Framework, United States Environmental Protection Agency, 2000.

781 Clarisse, L., Coheur, P. -F., Prata, F., Hadji-Lazaro, J., Hurtmans, D., and Clerbaux, C.: A
782 unified approach to infrared aerosol remote sensing and type specification, *Atmos.*
783 *Chem. Phys.*, 13, 2195-2221, 2013.

784 Cofala, J., Bertok, I., Borken-Kleefeld, J., Heyes, C., Klimont, Z., Rafaj, P., Sander, R.,
785 Schöpp, W., and Amann, M.: Emissions of Air Pollutants for the World Energy
786 Outlook 2012 Energy Scenarios, International Institute for Applied System Analysis
787 (IIASA), A-2361, Laxenburg, Austria, 2012.

788 Davis, J. M., Bhave, P. V., and Foley, K. M.: Parameterization of N₂O₅ reaction probabilities
789 on the surface of particles containing ammonium, sulfate, and nitrate, *Atmos. Chem.*
790 *Phys.*, 8, 5295-5311, 2008.

791 Dentener, F. J. and Crutzen, P. J.: Reaction of N₂O₅ on tropospheric aerosols: Impact on the
792 global distribution of NO_x, O₃, and OH levels, *J. Geophys. Res.*, 98, 7149-7163, 1993.

793 Emmons, L. K., Walters, S., Hess, P. G., Lamarque, J.-F., Pfister, G. G., Fillmore, D., Granier,
794 C., Guenther, A., Kinnison, D., Laepple, T., Orlando, J., Tie, X., Tyndall, G.,
795 Wiedinmyer, C., Baughcum, S. L., and Kloster, S.: Description and evaluation of the
796 Model for Ozone and Related chemical Tracers, version 4 (MOZART-4), *Geosci.*
797 *Model Dev.*, 3, 43-67, doi:10.5194/gmd-3-43-2010, 2010.

798 Eskes, H. J. and Boersma, K. F.: Averaging kernels for DOAS total-column satellite retrievals,
799 *Atmos. Chem. Phys.*, 3, 1285-1291, doi:10.5194/acp-3-1285-2003, 2003.

800 Evans, M. J. and Jacob, D. J.: Impact of new laboratory studies of N₂O₅ hydrolysis on global
801 model budgets of tropospheric nitrogen oxides, ozone, and OH, *Geophys. Res. Letts.*,
802 32, L09813, doi:10.1029/2005GL022469, 2005, 2005.

803 Fioletov, V. E., Bodeker, G. E., Miller, A. J., McPeters, R. D., and Stolarski, R.: Global and
804 zonal total ozone variations estimated from ground-based and satellite measurements:
805 1964-2000, *J. Geophys. Res.*, 107, D22, 4647, doi:10.1029/2001JD001350, 2002.

806 Fu, T., Jacob, D. J., Palmer, P. I., Chance, K., Wang, Y. X., Barletta, B., Blake, D. R., Staton, J.
807 C., and Pilling, M. J.: Space-based formaldehyde measurements as constrains on
808 volatile organic compound emissions in east and south Asia and implications for
809 ozone, *J. Geophys. Res.*, 112, D06312, doi:10.1029/2006JD007853, 2007.

810 Ghude, Sachin D., Pfister, Gabriele G., Jena, Chinmay, van der A, R. J., Emmons, Louisa K.,
811 and Kumar, Rajesh: Satellite constraints of nitrogen oxide (NO_x) emissions from India
812 based on OMI observations and WRF-Chem simulations, *Geophys. Res. Lett.*, 40, 1-6,
813 doi:10.1029/2012GL053926, 2013.

814 Han, K. M., Song, C. H., Ahn, H. J., Park, R. S., Woo, J. H., Lee, C. K., Richter, A.,
815 Burrows, J. P., Kim, J. Y., and Hong, J. H.: Investigation of NO_x emissions and NO_x-
816 related chemistry in East Asia using CMAQ-predicted and GOME-derived
817 NO₂ columns, *Atmos. Chem. Phys.*, 9, 1017-1036, doi:10.5194/acp-9-1017-2009,
818 2009.

819 Han, K. M., Lee, C. K., Lee, J., Kim, J. and Song, C. H.: A comparison study between model-
820 predicted and OMI-retrieved tropospheric NO₂ columns over the Korean peninsula,
821 *Atmos. Environ.*, 45, 2962-2971, 2011.

822 Han, K. M. and Song, C. H.: A budget analysis of NO_x column losses over the Korean
823 peninsula, *Asia-Pacific J. Atmos. Sci.*, 48(1), 55-65, 2012.

824 Han, K. M., Park, R. S., Kim, H. K., Woo, J. H., Kim, J., and Song, C. H.: Uncertainty in
825 biogenic isoprene emissions and its impacts on tropospheric chemistry in East Asia, *Sci.*
826 *Total Environ.*, vol. 463-464, 754-771, 2013.

827 Harris, G. W., Carter, W. P. L., Winer, A. M., Pitts, J. N., Platt, U., and Perner, D.:
828 Observations of nitrous acid in the Los Angeles atmosphere and implications for
829 predictions of ozone-precursor relationships, *Environ. Sci. Technol.*, 16(7), 414-419,
830 doi: 10.1021/es00101a009, 1982.

831 He, Y., Uno, I., Wang, Z., Ohara, T., Sugimoto, N., Shimizu, A., Richter, A., and Burrows, J.
832 P.: Variations of the increasing trend of tropospheric NO₂ over central east China
833 during the past decade, *Atmos. Environ.*, 41, 4865-4876, 2007.

834 Henderson, B. H., Pinder, R. W., Crooks, J., Cohen, R. C., Carlton, A. G., Pye, H. O. T., and
835 Vizuete, W.: Combining Bayesian methods and aircraft observations to constrain the
836 HO + NO₂ reaction rate, *Atmos. Chem. Phys.*, 12, 653-667, doi:10.5194/acp-12-653-
837 2012, 2012.

838 Herron-Thorpe, F. L., Lamb, B. K., Mount, G. H., and Vaughan, J. K.: Evaluation of a
839 regional air quality forecast model for tropospheric NO₂ columns using the OMI/Aura
840 satellite tropospheric NO₂ product, *Atmos. Chem. Phys.*, 10, 8839-8854,
841 doi:10.5194/acp-10-8839-2010, 2010.

842 Hilboll, A., Richter, A., and Burrows, J. P.: Long-term changes of tropospheric NO₂ over
843 megacities derived from multiple satellite instruments, *Atmos. Chem. Phys.*, 13, 4145-
844 4169, doi:10.5194/acp-13-4145-2013, 2013.

845 Hong, J. H., Lee, W. S., Kim, D. G., Lee, S. B., Kang, K. H.: 2006 Greenhouse gas and air
846 pollutants emissions in Korea, National Institute of Environmental Research (NIER),
847 Ministry of Environment of Korea, 2008.

848 Horowitz, L., Fiore, A. M., Milly, G. P., Cohen, R. C., Perring, A., Wooldridge, P. J., Hess, P.
849 G., Emmons, L. K., Lamarque, J. -F.: Observational constraints on the chemistry of
850 isoprene nitrates over the eastern United States, *J. Geophys. Res.*, 112, D12S08,
851 doi:10.1029/2006JD007747, 2007.

- 852 Hudman, R. C., Russell, A. R., Valin, L. C., and Cohen, R. C.: Interannual variability in soil
853 nitric oxide emissions over the United States as viewed from space, *Atmos. Chem.*
854 *Phys.*, 10, 9943-9952, doi:10.5194/acp-10-9943-2010, 2010.
- 855 Huijnen, V., Eskes, H. J., Poupkou, A., Elbern, H., Boersma, K. F., Foret, G., Sofiev, M.,
856 Valdebenito, A., Flemming, J., Stein, O., Gross, A., Robertson, L., D'Isidoro, M.,
857 Kioutsioukis, I., Friese, E., Amstrup, B., Bergstrom, R., Strunk, A., Vira, J.,
858 Zyryanov, D., Maurizi, A., Melas, D., Peuch, V.-H., and Zerefos, C.: Comparison of
859 OMI NO₂ tropospheric columns with an ensemble of global and European regional air
860 quality models, *Atmos. Chem. Phys.*, 10, 3273-3296, doi:10.5194/acp-10-3273-2010,
861 2010.
- 862 Itahashi, S., Uno, I., Irie, H., Kurokawa, J.-I., and Ohara, T.: Regional modeling of
863 tropospheric NO₂ vertical column density over East Asia during the period 2000–2010:
864 comparison with multisatellite observations, *Atmos. Chem. Phys.*, 14, 3623-3635,
865 doi:10.5194/acp-14-3623-2014, 2014.
- 866 Jacob, D. J.: Heterogeneous chemistry and tropospheric ozone, *Atmos. Environ.*, 34, 2131-
867 2159, 2000.
- 868 Jaeglé, L., Steinberger, L., Martin, R. V., and Chance, K.: Global partitioning of NO_x sources
869 using satellite observations: Relative roles of fossil fuel combustion, biomass burning
870 and soil emissions, *Faraday Discuss.*, 130, 407-423, doi:10.1039/b502128f, 2005.
- 871 Johnson, E. S., Bonjean, F., Lagerloef, G. S. E., and Gunn, J. T.: Validation and error analysis
872 of OSCAR sea surface currents, *J. Atmos. Oceanic Technol.*, 24, 688-701, 2007.
- 873 Karamchandani, P., Santos, L., Sykes, I., Zhang, Y., Tonne, C., and Seigneur, C.:
874 Development and evaluation of a state-of-the-science reactive plume model, *Environ.*
875 *Sci. Technol.*, 34, 870– 880, 2000.
- 876 Kim, H. S., Song, C. H., Park, R. S., Huey, G., and Ryu, J. Y.: Investigation of ship-plume
877 chemistry using a newly-developed photochemical/dynamic ship-plume model, *Atmos.*
878 *Chem. Phys.*, 9, 7531-7550, doi:10.5194/acp-9-7531-2009, 2009.
- 879 Kim, J.: GEMS (Geostationary Environment Monitoring Spectrometer) onboard the
880 GeoKOMPSAT to Monitor Air Quality in high Temporal and Spatial Resolution over
881 Asia-Pacific Region, EGU General Assembly 2012, 22-27 April 2012, Vienna, Austria,
882 p. 4051, 2012.
- 883 Kleipool, Q. L., Dobber, M. R., de Haan, J. F., and Levelt, P. E.: Earth surface reflectance
884 climatology from 3 years of OMI data, *J. Geophys. Res.*, 113, D18308,
885 doi:10.1029/2008JD010290, 2008.
- 886 Klimont, Z., Cofala, J., Xing, J., Wei, W., Zhang, C., Wang, S., Kejun, J., Bhandari, P., Mathur,
887 R., Purohit, P., Rafaj, P., Chambers, A., Amann, M., and Hao, J.: Projections of SO₂,
888 NO_x, and carbonaceous aerosols emissions in Asia, *Tellus*, 61B, 602-617, 2009.
- 889 Kubistin, D., Harder, H., Martinez, M., Rudolf, M., Sander, R., Bozem, H., Eerdeken, G.,
890 Fischer, H., Gurk, C., Klüpfel, T., Königstedt, R., Parchatka, U., Schiller, C. L.,
891 Stickler, A., Taraborrelli, D., Williams, J., and Lelieveld, J.: Hydroxyl radicals in the
892 tropical troposphere over the Suriname rainforest: comparison of measurements with
893 the box model MECCA, *Atmos. Chem. Phys.*, 10, 9705-9728, doi:10.5194/acp-10-
894 9705-2010, 2010.
- 895 Kurokawa, J., Ohara, T., Morikawa, T., Hanayama, S., Janssens-Maenhout, G., Fukui, T.,
896 Kawashima, K., and Akimoto, H.: Emissions of air pollutants and greenhouse gases
897 over Asian regions during 2000–2008: Regional Emission inventory in ASia (REAS)
898 version 2, *Atmos. Chem. Phys.*, 13, 11019-11058, doi:10.5194/acp-13-11019-2013,
899 2013.
- 900 Lamsal, L. N., Martin, R. V., van Donkelaar, A., Celarier, E. A., Bucsela, E. J., Boersma, K. F.,

901 Dirksen, R., Luo, C., and Wang, Y.: Indirect validation of tropospheric nitrogen
902 dioxide retrieved from the OMI satellite instrument: Insight into the seasonal variation
903 of nitrogen oxides at northern midlatitudes, *J. Geophys. Res.*, 115, D05302,
904 doi:10.1029/2009JD013351, 2010.

905 Lelieveld, J., Butler, T. M., Crowley, J. N., Dillon, T. J., Fischer, H., Ganzeveld, L., Harder, H.,
906 Lawrence, M. G., Martinez, M., Taraborrelli, D., and Williams, J.: Atmospheric
907 oxidation capacity sustained by a tropical forest, *Nature*, 452, 737-740,
908 doi:10.1038/nature06870, 2008.

909 Levelt, P. F., van den Oord, G. H. J., Dobber, M. R., Mälkki, A., Visser, H., de Vries, J.,
910 Stammes, P., Lundell, J. O. V., and Saari, H.: The Ozone Monitoring Instrument, *IEEE*
911 *Trans. Geosci. Remote Sens.*, vol. 44(5), 1093-1101, 2006.

912 Lin, J.-T., McElroy, M. B., and Boersma, K. F.: Constraint of anthropogenic NO_x emissions in
913 China from different sectors: a new methodology using multiple satellite retrievals,
914 *Atmos. Chem. Phys.*, 10, 63-78, doi:10.5194/acp-10-63-2010, 2010.

915 Lin, J.-T.: Satellite constraint for emissions of nitrogen oxides from anthropogenic, lightning
916 and soil sources over East China on a high-resolution grid, *Atmos. Chem. Phys.*, 12,
917 2881-2898, doi:10.5194/acp-12-2881-2012, 2012.

918 Lin, J.-T., Liu, Z., Zhang, Q., Liu, H., Mao, J., and Zhuang, G.: Modeling uncertainties for
919 tropospheric nitrogen dioxide columns affecting satellite-based inverse modeling of
920 nitrogen oxides emissions, *Atmos. Chem. Phys.*, 12, 12255-12275, doi:10.5194/acp-
921 12-12255-2012, 2012.

922 Ma, J., Richter, A., Burrows, J. P., Nüß, H., and van Aardenne, J. A.: Comparison of model-
923 simulated tropospheric NO₂ over China with GOME-satellite data, *Atmos. Environ.*,
924 40, 593-604, 2006.

925 Macintyre, H. L. and Evans, M. J.: Sensitivity of a global model to the uptake of N₂O₅ by
926 tropospheric aerosol, *Atmos. Chem. Phys.*, 10, 7409-7414, doi:10.5194/acp-10-7409-
927 2010, 2010.

928 Martin, R. V., Sioris, C. E., Chance, K., Ryerson, T. B., Bertram, T. H., Wooldridge, P. J.,
929 Cohen, R. C., Neuman, J. A., Swanson, A., and Flocke, F. M.: Evaluation of space-
930 based constraints on global nitrogen oxide emissions with regional aircraft
931 measurements over and downwind of eastern North America, *J. Geophys. Res.*, 111,
932 D15308, doi:10.1029/2005JD006680, 2006.

933 McConnell, J. C., and McElroy, M. B.: Odd nitrogen in the atmosphere, *J. Atmos. Sci.*, 30(8),
934 1465-1480, 1973.

935 Mijling, B., van der A, R. J., and Zhang, Q.: Regional nitrogen oxides emission trends in East
936 Asia observed from space, *Atmos. Chem. Phys.*, 13, 12003-12012, doi:10.5194/acp-
937 13-12003-2013, 2013.

938 Mollner, A. K., Valluvadasan, S., Feng, L., Sprague, M. K., Okumura, M., Milligan, D. B.,
939 Bloss, W. J., Sander, S. P., Martien, P. T., Harley, R. A., McCoy, A. B., and Carter, W. P.
940 L.: Rate of Gas Phase Association of Hydroxyl Radical and Nitrogen Dioxide, *Science*,
941 330, 646-649, doi:10.1126/science.1193030, 2010.

942 Monaghan, A. J., Bromwich, D. H., and Wang, S. H.: Recent trends in Antarctic snow
943 accumulation from Polar MM5 simulations, *Phil. Trans. R. Soc. A*, 364, 1683-1708,
944 doi:10.1098/rsta.2006.1795, 2006.

945 Müller, J.-F., Stavrou, T., Wallens, S., De Smedt, I., Van Roozendaal, M., Potosnak, M. J.,
946 Rinne, J., Munger, B., Goldstein, A., and Guenther, A. B.: Global isoprene emissions
947 estimated using MEGAN, ECMWF analyses and a detailed canopy environment
948 model, *Atmos. Chem. Phys.*, 8, 1329-1341, doi:10.5194/acp-8-1329-2008, 2008.

949 Ohara, T., Akimoto, H., Kurokawa, J., Horii, N., Yamaji, K., Yan, X., and Hayasaka, T.: An

950 Asian emission inventory of anthropogenic emission sources for the period 1980-2020,
951 Atmos. Chem. Phys., 7, 4419-4444, 2007.

952 Pagsberg, P., Bjergbakke, E., Ratajczak, E., and Sillescu, A.: Kinetics of the gas phase
953 reaction $\text{OH} + \text{NO}(+\text{M}) \rightarrow \text{HONO}(+\text{M})$ and the determination of the UV absorption
954 cross sections of HONO, Chem. Phys. Lett., 272, 383-390, 1997.

955 Park, R. S., Han, K. M., Song, C. H., Park, M. E., Lee, S. J., Hong, S. Y., Kim, J., and Woo, J.
956 -H.: Current Status and Development of Modeling Techniques for Forecasting and
957 Monitoring of Air Quality over East Asia, J. KOSAE (in Korean), 29(4), 407-438,
958 2013.

959 Park, R.S., Lee, S., Shin, S.-K., and Song, C.H.: Contribution of ammonium nitrate to aerosol
960 optical depth and direct radiative forcing by aerosols over East Asia, Atmos. Chem.
961 Phys., 14, 2185-2201, 2014.

962 Platt, U. F., Winer, A. M., Biermann, H. W., Atkinson, R., and Pitts, J. N.: Measurement of
963 nitrate radical concentrations in continental air, Environ. Sci. Technol., 18(5), 365-369,
964 doi:10.1021/es00123a015, 1984.

965 Pleim, J. E.: A combined local and nonlocal closure model for the atmospheric boundary layer,
966 Part I: Model description and testing, J. Appl. Meteor. Climatol., 46, 1383-1395, 2007.

967 Pugh, T. A. M., MacKenzie, A. R., Hewitt, C. N., Langford, B., Edwards, P. M.,
968 Furneaux, K. L., Heard, D. E., Hopkins, J. R., Jones, C. E., Karunaharan, A., Lee, J.,
969 Mills, G., Misztal, P., Moller, S., Monks, P. S., and Whalley, L. K.: Simulating
970 atmospheric composition over a South-East Asian tropical rainforest: performance of a
971 chemistry box model, Atmos. Chem. Phys., 10, 279-298, doi:10.5194/acp-10-279-
972 2010, 2010.

973 Richter, A., Burrows, J. P., Nüß, H., Granier, C., and Niemeier, U.: Increase in tropospheric
974 nitrogen dioxide over China observed from space, Nature, 437, 129-132, 2005.

975 Richter, A., Begoin, M., Hilboll, A., and Burrows, J. P.: An improved NO_2 retrieval for the
976 GOME-2 satellite instrument, Atmos. Meas. Tech., 4, 1147-1159, 2011.

977 Riemer, N., Vogel, H., Vogel, B., Schell, B., Ackermann, I., Kessler, C., and Hass, H.: Impact
978 of the heterogeneous hydrolysis of N_2O_5 on chemistry and nitrate aerosol formation in
979 the lower troposphere under photochemical conditions, J. Geophys. Res., 108(D4), 4144,
980 doi:10.1029/2002JD002436, 2003.

981 Roberts, J. M., Flocke, F., Stroud, C. A., Hereid, D., Williams, E. J., Fehsenfeld, F. C., Brune,
982 W., Martinez, M., and Harder, H.: Ground-based measurements of peroxyacetylic
983 nitric anhydrides (PANs) during the 1999 Southern Oxidant Study Nashville Intensive,
984 J. Geophys. Res., 107(d21), 4554, doi:10.1029/2001JD000947, 2002.

985 Rodgers, C. D.: Inverse methods for atmospheric sounding: theory and practice, Series on
986 Atmospheric, Oceanic and Planetary Physics – Vol. 2, World Scientific Publishing,
987 Singapore, 43-63, 2000.

988 Rondon, A. and Sanhueza, E.: High HONO atmospheric concentrations during vegetation
989 burning in the tropical savannah, Tellus B, 41B(4), 474-477, doi: 10.1111/j.1600-
990 0889.1989.tb00323.x, 1989.

991 Sander, S. P., Abbatt, J., Barker, J. R., Burkholder, J. B., Friedl, R. R., Golden, D. M., Huie, R.
992 E., Kolb, C. E., Kurylo, M. J., Moortgat, G. K., Orkin, V. L., and Wine, P. H.:
993 Chemical Kinetics and Photochemical Data for Use in Atmospheric Studies,
994 Evaluation number 17, NASA Panel for data evaluation, JPL Publication 10-6, Jet
995 Propulsion Laboratory, Pasadena, <http://jpldataeval.jpl.nasa.gov> (last access: 27 June
996 2014), 2011.

997 Schneider, P. and van der A, R. J.: A global single-sensor analysis of 2002-2011 tropospheric
998 nitrogen dioxide trends observed from space, J. Geophys. Res., 117, D16309,

999 doi:10.1029/2012JD017571, 2012.

1000 Shi, C., Fernando, Wang, Z., An, X., and Wu, Q.: Tropospheric NO₂ columns over East
1001 Central China: Comparisons between SCIAMACHY measurements and nested
1002 CMAQ simulations, *Atmos. Environ.*, 42, 7165-7173, 2008.

1003 Song, C. H., Chen, G., Hanna, S. R., Crawford, J., and Davis, D. D.: Dispersion and chemical
1004 evolution of ship plumes in the marine boundary layer: Investigation of O₃/NO_y/HO_x
1005 chemistry, *J. Geophys. Res.*, 108(D4), 4143, doi:10.1029/2002JD002216, 2003

1006 Song, C. H., Kim, H. S., von Glasow, R., Brimblecombe, P., Kim, J., Park, R. J., Woo, J. H.,
1007 and Kim, Y. H.: Source identification and budget analysis on elevated levels of
1008 formaldehyde within the ship plumes: a ship-plume photochemical/dynamic model
1009 analysis, *Atmos. Chem. Phys.*, 10, 11969-11985, doi:10.5194/acp-10-11969-2010,
1010 2010.

1011 Sörgel, M., Regelin, E., Bozem, H., Diesch, J.-M., Drewnick, F., Fischer, H., Harder, H.,
1012 Held, A., Hosaynali-Beygi, Z., Martinez, M., and Zetzsch, C.: Quantification of the
1013 unknown HONO daytime source and its relation to NO₂, *Atmos. Chem. Phys.*, 11,
1014 10433-10447, doi:10.5194/acp-11-10433-2011, 2011.

1015 Stauffer, D. R. and Seaman, N. L.: Use of four-dimensional data assimilation in a limited-area
1016 mesoscale model. Part I: experiments with synoptic-scale data, *Monthly Weather
1017 Review*, 118 (6), 1250-1277, 1990.

1018 Stauffer, D. L. and Seaman, N. L., Multiscale four-dimensional data assimilation, *J. Applied
1019 Meteorology*, 33 (3), 416-434, 1994.

1020 Stavrou, T., Müller, J. -F., Boersma, K. F., De Smedt, I., and van der A, R. J.: Assessing the
1021 distribution and growth rates of NO_x emission sources by inverting a 10-year record of
1022 NO₂ satellite columns, *Geophys. Res. Lett.*, 35, L10801, doi:10.1029/2008GL033521,
1023 2008.

1024 Stavrou, T., Müller, J.-F., Boersma, K. F., van der A, R. J., Kurokawa, J., Ohara, T., and
1025 Zhang, Q.: Key chemical NO_x sink uncertainties and how they influence top-down
1026 emissions of nitrogen oxides, *Atmos. Chem. Phys.*, 13, 9057-9082, doi:10.5194/acp-
1027 13-9057-2013, 2013.

1028 Stemmler, K., Ammann, M., Donders, C., Kleffmann, J., and George, C.: Photosensitized
1029 reduction of nitrogen dioxide on humic acid as a source of nitrous acid, *Nature*, 440,
1030 195-198, doi:10.1038/nature04603, 2006.

1031 Streets, D. G., Bond, T. C., Carmichael, G. R., Fernandes, S. D., Fu, Q., He, D., Klimont, Z.,
1032 Nelson, S. M., Tsai, N. Y., Wang, M. Q., Woo, J. -H., and Yarber, K. F.: An inventory
1033 of gaseous and primary aerosol emissions in Asia in the year 2000, *J. Geophys. Res.*,
1034 108 (D21), 8809, doi:10.1029/2002JD003093, 2003.

1035 Svensson, R., Ljungström, E., and Lindqvist, O.: Kinetics of the reaction between nitrogen
1036 dioxide and water vapour, *Atmos. Environ.*, 21(7), 1529-1539, 1987.

1037 Tie, X., Emmons, L., Horowitz, L., Brasseur, G., Ridley, B., Atlas, E., Stround, C., Hess, P.,
1038 Klonecki, A., Madronich, S., Talbot, R., and Dibb, J.: Effect of sulfate aerosol on
1039 tropospheric NO_x and ozone budgets: Model simulations and TOPSE evidence, *J.
1040 Geophys. Res.*, 108(D4), 8364, doi: 10.1029/2001JD001508, 2003.

1041 Uno, I., He, Y., Ohara, T., Yamaji, K., Kurokawa, J.-I., Katayama, M., Wang, Z., Noguchi, K.,
1042 Hayashida, S., Richter, A., and Burrows, J. P.: Systematic analysis of interannual and
1043 seasonal variations of model-simulated tropospheric NO₂ in Asia and comparison with
1044 GOME-satellite data, *Atmos. Chem. Phys.*, 7, 1671-1681, 2007.

1045 van der A, R. J., Peters, D. H. M. U., Eskes, H., Boersma, K. F., Van Roozendaal, M., De
1046 Smedt, I., and Kelder, H. M., Detection of the trend and seasonal variation in
1047 tropospheric NO₂ over China, *J. Geophys. Res.*, 111 (D12), 27, DOI:

1048 10.1029/2005JD006594, 2006.
1049 Wang, Y., McElory, M. B., Martin, R. V., Streets, D. G., Zhang, Q., and Fu, T.-M.: Seasonal
1050 variability of NO_x emissions over east China constrained by satellite observations:
1051 Implications for combustion and microbial sources, *J. Geophys. Res.*, 112, D06301,
1052 doi:10.1029/2006JD007538, 2007.
1053 Wild, O., Prather, M. J., and Akimoto, H.: Indirect long-term global radiative cooling from
1054 NO_x emissions, *Geophys. Res. Lett.*, 28(9), 1719-1722, 2001.
1055 Willmott, C. J.: On the validation of models, *Phys. Geogr.*, 2, 184-194, 1981.
1056 Xing, J., Wang, S. X., Chatani, S., Zhang, C. Y., Wei, W., Hao, J. M., Klimont, Z., Cofala, J.,
1057 and Amann, M.: Projections of air pollutant emissions and its impacts on regional air
1058 quality in China in 2020, *Atmos. Chem. Phys.*, 11, 3119-3136, doi:10.5194/acp-11-
1059 3119-2011, 2011.
1060 Yamartino, R. J.: Nonnegative, conserved scalar transport using grid-cell-centered, spectrally
1061 constrained Blackman cubics for applications on a variable-thickness mesh, *Mon. Wea.*
1062 *Rev.*, 121, 753-763, 1993.
1063 Zhang, Q., Streets, D. G., He, K., Wang, Y., Richter, A., Burrows, J. P., Uno, I., Jang, C. J.,
1064 Chen, D., Yao, Z., and Lei, Y.: NO_x emission trends for China, 1995-2004: The view
1065 from the ground and the view from space, *J. Geophys. Res.*, 112, D22306,
1066 doi:10.1029/2007JD008684, 2007.
1067 Zhang, Q., Streets, D. G., Carmichael, G. R., He, K. B., Huo, H., Kannari, A., Klimont, Z.,
1068 Park, I. S., Reddy, S., Fu, J. S., Chen, D., Duan, L., Lei, Y., Wang, L. T., and Yao, Z. L.:
1069 Asian emissions in 2006 for the NASA INTEX-B mission, *Atmos. Chem. Phys.*, 9,
1070 5131-5153, doi:10.5194/acp-9-5131-2009, 2009.
1071 Zhou, X., Zhang, N., TerAvest, M., Tang, D., Hou, J., Bertman, S., Alaghmand, M., Shepson,
1072 P. B., Carroll, M. A., Griffith, S., Dusanter, S., and Stevens, P. S.: Nitric acid
1073 photolysis on forest canopy surface as a source for tropospheric nitrous acid, *Nature*
1074 *Geoscience*, 4, 440-443, doi:10.1038/ngeo1164, 2011.
1075 Zyrichidou, I., Koukouli, M. E., Balis, D. S., Kioutsioukis, I., Poupkou, A., Katragkou, E.,
1076 Melas, D., Boersma, K. F., and van Roozendaal, M.: Evaluation of high resolution
1077 simulated and OMI retrieved tropospheric NO₂ column densities over Southeastern
1078 Europe, *Atmos. Res.*, 122, 55-65, 2013.
1079

1080 **Figure Captions**

1081

1082 **Fig. 1.** Monthly variation in NO_x emissions in China. Here, the ‘MEIC_2008’ and
1083 ‘MEIC_2010’ were obtained from the website, <http://www.meicmodel.org/>.

1084

1085 **Fig. 2.** Study domain and eight focus regions in this study: Central East China (CEC), Central
1086 East China 2 (CEC2), South China (SC), Sichuan Basin (SB), South Korea (SK),
1087 western part of Japan (JP1), eastern part of Japan (JP2), and entire domain (DM).

1088

1089 **Fig. 3.** Vertical distributions of averaging kernels (AKs) with error bars (one-sigma standard
1090 deviations from the mean) for four seasons over (a) CEC, (b) CEC2, (c) SC, (d) SB, (e)
1091 SK, (f) JP1, (g) JP2, and (h) DM regions (refer to Fig. 2 regarding the regions of
1092 analysis).

1093

1094 **Fig. 4.** Flow diagram for direct comparison between CMAQ-estimated and OMI-retrieved
1095 NO₂ columns.

1096

1097 **Fig. 5.** Spatial and seasonal distributions of CMAQ-calculated tropospheric NO₂ columns (a)
1098 without the applications of the AKs and (b) with the AKs and (c) OMI-retrieved NO₂
1099 columns from the KNMI algorithm. Differences between OMI-retrieved and CMAQ-
1100 calculated NO₂ columns (d) before the applications of the AKs and (e) after the
1101 applications of the AKs.

1102

1103 **Fig. 6.** Seasonal scatter plots between CMAQ-calculated and OMI-retrieved NO₂ columns
1104 (Unit: $\times 10^{15}$ molecules cm⁻²) using seasonally averaged data sets over the CEC, CEC2,
1105 SC, SB, SK, JP1, JP2, and DM regions. Here, the AKs were applied to the CMAQ
1106 model simulations. R, S, Y-I, and N represent the correlation coefficient, linear
1107 regression slope, y-intercept, and the number of data points, respectively.

1108

1109 **Fig. 7.** Statistical analyses between CMAQ-calculated and OMI-retrieved NO₂ columns using
1110 the performance metrics defined in Table A1. Here, the color bars represent ME and
1111 MB at the top, MNGE, MNB, NME, NMB, MFE, and MFB in the middle, and IOA
1112 and R at the bottom. Here, light colors show good agreements while dark colors
1113 indicate poor agreements.

1114

1115 **Fig. 8.** Spatial distributions of (a) CMAQ-calculated NO₂ columns with the AKs and (b)
1116 OMI-retrieved NO₂ columns and (c) their differences for four seasonal episodes. Here,
1117 the monthly variations of NO_x emissions from Han et al. (2009) were applied to the
1118 CMAQ model simulations.

1119

1120 **Fig. 9.** CMAQ-calculated NO₂ columns using (a) INTEX-B inventory and (b) REAS
1121 inventory over China and (c) OMI-observed NO₂ columns for January.

1122

1123 **Fig. 10.** CMAQ-calculated NO₂ columns using five $\gamma_{\text{N}_2\text{O}_5}$ parameterizations from (a)
1124 Dentener and Crutzen (1993), (b) Riemer et al. (2003), (c) combination of Riemer et al.
1125 (2003) and Evans and Jacob (2005), (d) Davis et al. (2008), and (e) Brown et al.,
1126 (2006) and (f) OMI-observed NO₂ columns for January.

1127

1128 **Fig. S1.** Scatter plots between daily $\Omega_{\text{CMAQ,AK}}$ and daily Ω_{OMI} over the DM regions for four

1129 seasonal episodes.

1130 **Fig. S2.** As in Fig. 6, except for the monthly variations of NO_x emissions from Han et al.
1131 (2009).

1132

1133 **Fig. S3.** As in Fig. 7, except for the monthly variations of NO_x emissions from Han et al.
1134 (2009).

1135

1136

Table 1. Description of CMAQ model simulations conducted in this study.

Cases	Sensitivity test	Month, year	Description	Section
1	Base-case simulation	Jan. – Dec., 2006	- Seasonal variation of NO _x emission from INTEX-B inventory for China (Zhang et al., 2009) and from Han et al. (2009) for Korea and Japan. - NO _x emissions from INTEX-B, CAPSS, and REAS inventories for China, Korea, and Japan, respectively - Parameterization of $\gamma_{\text{N}_2\text{O}_5}$ from the combination of Riemer et al. (2003) and Evans and Jacob (2005)	Sect. 3.1
2	Seasonal variation of NO _x emission	Jan. – Dec., 2006	- As case 1 except for seasonal variation of NO _x emission from Han et al. (2009) for China (i.e. all the monthly factors from Han et al. (2009) for China, Korea, and Japan.)	Sect. 3.2.1
3	Emission strength	Jan., 2006	- As case 1 except for NO _x emissions from REAS inventory for China	Sect. 3.2.2
4	Reaction probability of N ₂ O ₅	Jan., 2006	- As case 1 except for the $\gamma_{\text{N}_2\text{O}_5}$ parameterizations from: (i) Dentener and Crutzen (1993); (ii) Riemer et al. (2003); (iii) Davis et al. (2008); and (iv) Brown et al., (2006)	Sect. 3.2.3

Table 2. Average tropospheric NO₂ columns, standard deviations, and the normalized mean error (NME) with and without the application of AKs for four seasons.

Region	Season	n ⁽¹⁾	Ω_{CMAQ} (w/o AKs) ⁽²⁾	$\Omega_{\text{CMAQ,AK}}$ (w/ AKs) ⁽²⁾	Ω_{OMI} ⁽²⁾	NME (w/o AKs)	NME (w/ AKs)
CEC	Spring	900	11.68 (6.19) ⁽³⁾	6.40 (3.95) ⁽³⁾	6.89 (4.07)	74.48	29.48
	Summer	900	6.43 (4.09)	2.60 (1.80)	5.29 (3.02)	45.55	53.06
	Fall	900	13.29 (7.71)	7.18 (5.04)	9.49 (5.89)	52.08	32.79
	Winter	900	16.95 (9.52)	11.08 (7.52)	14.18 (8.05)	37.52	31.77
CEC2	Spring	820	10.49 (6.34)	4.79 (4.12)	4.45 (3.98)	135.72	29.75
	Summer	820	6.01 (6.16)	2.31 (2.92)	3.02 (2.15)	102.70	39.44
	Fall	820	12.36 (7.44)	5.84 (4.39)	4.97 (3.97)	148.85	36.61
	Winter	820	20.07 (6.84)	11.24 (5.54)	8.49 (5.79)	136.26	42.58
SC	Spring	1125	3.79 (2.87)	1.16 (1.04)	2.20 (2.03)	81.80	50.26
	Summer	1124	2.65 (2.57)	0.76 (0.85)	1.77 (1.73)	65.26	57.83
	Fall	1125	3.79 (2.79)	1.27 (1.02)	2.20 (2.31)	79.89	44.80
	Winter	1125	8.98 (4.06)	3.21 (1.88)	3.24 (3.39)	181.26	36.41
SB	Spring	408	4.25 (2.84)	1.53 (1.09)	2.56 (1.55)	80.16	44.97
	Summer	420	2.34 (1.66)	0.78 (0.59)	2.14 (0.99)	39.86	63.31
	Fall	418	6.37 (4.47)	2.34 (1.76)	2.71 (2.15)	143.93	43.75
	Winter	403	11.55 (7.69)	5.31 (4.14)	3.43 (3.01)	237.75	72.46
SK	Spring	260	9.14 (5.78)	4.95 (3.50)	5.24 (3.74)	75.37	26.93
	Summer	260	7.52 (7.94)	3.06 (3.60)	3.41 (2.58)	128.05	42.73
	Fall	260	8.85 (6.60)	4.60 (3.71)	4.81 (3.62)	93.57	38.81
	Winter	260	12.30 (5.69)	6.82 (3.37)	6.68 (4.14)	88.42	29.78
JP1	Spring	204	4.61 (1.51)	2.03 (0.73)	3.58 (2.48)	44.83	45.50
	Summer	204	2.47 (1.06)	0.77 (0.33)	2.91 (1.98)	34.88	73.42
	Fall	204	4.62 (1.92)	1.91 (0.90)	3.57 (2.50)	41.81	48.26
	Winter	204	7.63 (2.88)	3.47 (1.41)	4.48 (3.07)	74.66	36.95
JP2	Spring	285	3.90 (3.27)	1.72 (1.75)	3.09 (2.96)	36.19	45.69
	Summer	286	2.41 (2.08)	0.86 (0.81)	2.64 (2.77)	29.99	67.72
	Fall	286	3.96 (3.33)	1.63 (1.66)	3.12 (3.17)	31.95	47.71
	Winter	279	5.84 (4.60)	2.56 (2.45)	3.92 (4.20)	55.64	42.72
Entire domain	Spring	15175	3.02 (4.46)	1.35 (2.39)	1.97 (2.43)	80.49	45.85
	Summer	15207	1.76 (3.09)	0.64 (1.29)	1.59 (1.72)	59.27	63.15
	Fall	15224	3.31 (5.13)	1.45 (2.72)	2.06 (3.05)	78.78	44.27
	Winter	14075	5.97 (7.31)	2.96 (4.52)	3.20 (4.79)	98.13	40.31

⁽¹⁾ The number of data; ⁽²⁾ Unit, $\times 10^{15}$ molecules cm^{-2} ; ⁽³⁾ Standard deviations of the distributions of tropospheric NO₂ columns

Table 3. Reaction probabilities of N₂O₅ onto aerosol surfaces.

References	Condensing medium	Reaction probability of N ₂ O ₅ ($\gamma_{N_2O_5}$)
Dentener and Crutzen (1993) [†] (Scheme I Fig. 10 (a))	Aqueous particles	$\gamma_{N_2O_5} = 0.1$
Jacob (2000) ^{†,‡}	Aqueous particles	$\gamma_{N_2O_5} = 0.1$ (Range: 0.01-1)
Tie et al. (2003) [†]	Aqueous particles	$\gamma_{N_2O_5} = 0.04$ (Range: 0.0-0.10)
Riemer et al. (2003) [†] (Scheme II in Fig. 10 (b))	Sulfate and Nitrate	$\gamma_{N_2O_5} = f \cdot \gamma_1 + (1-f) \cdot \gamma_2$ (Range: 0.02 - 0.002) $\gamma_1 = 0.02, \gamma_2 = 0.002; f = \frac{m_{SO_4^{2-}}}{m_{SO_4^{2-}} + m_{NO_3^-}}$ $m_{SO_4^{2-}}$ and $m_{NO_3^-}$: aerosol mass concentrations of sulfate and nitrate, respectively
Evans and Jacob (2005) [†]	Sulfate	$\gamma_{N_2O_5} = \alpha \times 10^\beta$ $\alpha = 2.79 \times 10^{-4} + 1.3 \times 10^{-4} \times RH - 3.43 \times 10^{-6} \times RH^2 + 7.52 \times 10^{-8} \times RH^3$ $\beta = 4 \times 10^{-2} \times (294 - T)$ (T ≥ 282K) $\beta = 0.48$ (T < 282K)
	OC	$\gamma_{N_2O_5} = RH \times 5.2 \times 10^{-4}$ (RH < 57%) $\gamma_{N_2O_5} = 0.03$ (RH ≥ 57%)
	BC	$\gamma_{N_2O_5} = 0.005$
	Sea salt	$\gamma_{N_2O_5} = 0.005$ (RH < 62%) $\gamma_{N_2O_5} = 0.03$ (RH ≥ 62%)
	Dust	$\gamma_{N_2O_5} = 0.01$
		RH : fractional relative humidity; T : temperature (K)
Combination of parameterization by Evans and Jacob (2005) and Riemer et al. (2003) [†] (Scheme III in Fig. 10 (c))	Sulfate and Nitrate	$\gamma_{N_2O_5} = f \cdot \gamma_1 + (1-f) \cdot \gamma_2$ $\alpha = 2.79 \times 10^{-4} + 1.3 \times 10^{-4} \times RH - 3.43 \times 10^{-6} \times RH^2 + 7.52 \times 10^{-8} \times RH^3$ $f = \frac{m_{SO_4^{2-}}}{m_{SO_4^{2-}} + m_{NO_3^-}}$ $\gamma_1 = \alpha \times 10^{0.48}; \gamma_2 = 0.1 \times \gamma_1$ (T < 282K)

		$\gamma_1 = \alpha \times 10^\beta$; $\gamma_2 = 0.1 \times \gamma_1$; $\beta = 4 \times 10^{-2} \times (294 - T)$ (T \geq 282K)
Davis et al. (2008) [†] (Scheme IV in Fig. 10 (d))	Aqueous particles	$\gamma_{N_2O_5, mix} = \sum_{i=1}^3 x_i \cdot \gamma_i$ $x_1 = 1 - (x_2 + x_3) \quad \text{for bisulfate}$ $x_2 = \max\left(0, \min\left(1 - x_3, \frac{c_{Ammo}}{c_{Nit} + c_{Sulf}} - 1\right)\right) \quad \text{for sulfate}$ $x_3 = \frac{c_{Nit}}{c_{Nit} + c_{Sulf}} \quad \text{for nitrate}$
	Bisulfate (i=1)	$\lambda_1 = -4.559088 + 2.8593 \times RH - 0.111201 \times T_{287}$; $\gamma_1 = \min\left(\frac{1}{1 + e^{-\lambda_1}}, 0.08585\right)$
	Sulfate (i=2)	$\lambda_2 = \lambda_1 - 0.369769$; $\gamma_2 = \min\left(\frac{1}{1 + e^{-\lambda_2}}, 0.053\right)$
	Nitrate (i=3)	$\lambda_3 = -0.8107744 + 4.9017 \times RH$; $\gamma_3 = \min\left(\frac{1}{1 + e^{-\lambda_3}}, 0.0154\right)$
		c_{Ammo} , c_{Nit} , and c_{Sulf} : molar concentration of ammonium, nitrate, and sulfate, respectively
	Dry particles	$\gamma_{N_2O_5, mix} = (x_1 + x_2)\gamma_d + x_3 \times \min(\gamma_d, \gamma_3)$ $\lambda_d = -6.133764 + 3.5920 \times RH - 0.196879 \times T_{293}$; $\gamma_d = \min\left(\frac{1}{1 + e^{-\lambda_d}}, 0.0124\right)$
Brown et al. (2006) [‡] (Scheme V in Fig. 10 (e))		$\gamma_{N_2O_5} = \frac{4k_{N_2O_5}}{c_{mean}A}$ <ul style="list-style-type: none"> i) 0.017 ± 0.004 (over Ohio and western Pennsylvania, US) ii) < 0.0010 (over eastern Pennsylvania and New Jersey, US) iii) < 0.0016 (over New York, US) $k_{N_2O_5}$: rate constant (s ⁻¹); c_{mean} : mean molecular speed of N ₂ O ₅ (cm s ⁻¹); A : aerosol surface density (μm ² cm ⁻³)

[†] Modeling study; [‡] Measurement study.

Table 4. Average tropospheric NO₂ columns, standard deviations and the ratios of the $\Omega_{\text{CMAQ,AK}}$ to the Ω_{OMI} , when different γ_{N2O5} parameterizations were applied to the CMAQ model simulations for January.

Region	Scheme ⁽¹⁾	n ⁽²⁾	$\Omega_{\text{CMAQ,AK}}$ ⁽³⁾	Ω_{OMI} ⁽³⁾	R= $\Omega_{\text{CMAQ,AK}} / \Omega_{\text{OMI}}$
CEC	Scheme I	896	11.11 (8.49) ⁽⁴⁾	13.3292 (9.00)	0.78
	Scheme II		12.40 (9.42)		0.87
	Scheme III		12.32 (9.35)		0.86
	Scheme IV		12.21 (9.27)		0.85
	Scheme V		14.23 (10.08)		0.99
CEC2	Scheme I	820	9.78 (6.14)	8.05 (6.34)	1.21
	Scheme II		11.37 (6.77)		1.41
	Scheme III		11.43 (6.82)		1.42
	Scheme IV		11.24 (6.74)		1.40
	Scheme V		13.53 (7.70)		1.68
SC	Scheme I	1125	2.47 (1.75)	2.98 (3.09)	0.83
	Scheme II		2.88 (1.88)		0.96
	Scheme III		2.80 (1.83)		0.94
	Scheme IV		2.77 (1.82)		0.93
	Scheme V		3.44 (2.06)		1.15
SB	Scheme I	386	5.05 (4.43)	3.34 (2.55)	1.51
	Scheme II		5.68 (4.83)		1.70
	Scheme III		5.43 (4.63)		1.63
	Scheme IV		5.44 (4.65)		1.63
	Scheme V		6.78 (5.65)		2.03
SK	Scheme I	260	6.80 (3.71)	6.70 (4.64)	1.01
	Scheme II		7.43 (3.83)		1.11
	Scheme III		7.29 (3.79)		1.09
	Scheme IV		7.26 (3.79)		1.08
	Scheme V		8.42 (4.03)		1.26
JP1	Scheme I	202	3.51 (1.75)	4.35 (2.58)	0.81
	Scheme II		3.96 (1.92)		0.91
	Scheme III		3.80 (1.86)		0.87
	Scheme IV		3.81 (1.87)		0.88
	Scheme V		4.34 (2.03)		1.00
JP2	Scheme I	192	2.69 (2.60)	4.68 (4.60)	0.57
	Scheme II		2.89 (2.73)		0.62
	Scheme III		2.81 (2.67)		0.60
	Scheme IV		2.82 (2.68)		0.60
	Scheme V		3.18 (2.84)		0.68
Entire domain	Scheme I	12901	2.88 (4.82)	3.23 (5.14)	0.89
	Scheme II		3.27 (5.40)		1.01
	Scheme III		3.22 (5.38)		1.00
	Scheme IV		3.20 (5.33)		0.99
	Scheme V		3.82 (6.22)		1.18

⁽¹⁾ Scheme I (Dentener and Crutzen, 1993), Scheme II (Riemer et al., 2003), Scheme III (combination of Riemer et al., 2003 and Evans and Jacob, 2005), Scheme IV (Davis et al., 2007), Scheme V (Brown et al., 2006); ⁽²⁾ The number of data; ⁽³⁾ Unit, $\times 10^{15}$ molecules cm^{-2} ; ⁽⁴⁾ Standard deviations of the distributions of tropospheric NO₂ columns

Table 5. Relative changes in the CMAQ-calculated NO₂ columns for several case studies, compared to those from the standard case simulation (Case 1).

Case	Sensitivity test	Season	Relative change ⁽¹⁾ (%)								
			CEC	CEC2	SC	SB	SK	JP1	JP2	DM	
2	NO _x seasonal variation (Han et al., 2009)	Spring	33.46	32.44	38.47	32.65	(15.31) ⁽²⁾	(10.94)	(6.68)	{30.67} ⁽³⁾	
		Summer	-31.16	-28.99	-26.37	-26.42	(-1.40)	(-1.44)	(-1.00)	{-21.96}	
		Fall	-21.74	-23.05	-23.90	-21.97	(-2.12)	(-1.20)	(-0.84)	{-18.67}	
		Winter	21.25	22.34	22.99	65.37	(12.95)	(8.04)	(7.36)	{23.30}	
3	Emission strength (REAS v1.11)	Jan.	-32.55	-48.32	-31.45	-58.44	(-0.72)	(27.04)	(-1.02)	{-30.49}	
4	γ _{N2O5}	(Scheme I: Dentener and Crutzen, 1993)	Jan.	-9.76	-14.43	-11.71	-7.13	-6.74	-7.51	-4.32	-10.84
		(Scheme II: Riemer et al., 2003)	Jan.	0.72	-0.54	2.69	4.54	1.91	4.23	2.87	1.52
		(Scheme IV: Davis et al., 2008)	Jan.	-0.85	-1.60	-1.08	0.04	-0.33	0.37	0.38	-0.87
		(Scheme V: Brown et al., 2006)	Jan.	15.59	18.44	22.72	24.76	15.57	14.17	13.02	18.52

$$^{(1)} \text{ Relative change (\%)} = \frac{\Omega_{CASE,i} - \Omega_{CASE,1}}{\Omega_{CASE,1}} \times 100$$

^{(2), (3)} Since the sensitivity parameters were applied only to China for the case 2 and 3 simulations, the relative changes in the parentheses over the SK, JP1, and JP2 regions indicate indirect impacts caused by long-range transports of the changes from China. The relative changes in the brackets in the entire domain (DM region) also include such indirect impacts from China.

Table S1. As Table 2, except for applying the seasonal variations of NO_x emission fluxes from Han et al. (2009) to the CMAQ model simulations.

Region	Season	n ⁽¹⁾	Ω _{CMAQ} (w/o AKs) ⁽²⁾	Ω _{CMAQ,AK} (w/ AKs) ⁽²⁾	Ω _{OMI} ⁽²⁾	NME (w/o AKs)	NME (w/ AKs)
CEC	Spring	900	15.28 (7.98) ⁽³⁾	8.54 (5.20) ⁽³⁾	6.89 (4.07) ⁽³⁾	143.17	43.31
	Summer	900	4.44 (2.76)	1.79 (1.21)	5.29 (3.02)	35.70	66.29
	Fall	900	10.41 (6.15)	5.62 (4.00)	9.49 (5.89)	37.26	41.58
	Winter	900	20.22 (11.19)	13.44 (9.08)	14.18 (8.05)	63.21	33.44
CEC2	Spring	820	13.85 (7.47)	6.35 (4.95)	4.45 (3.98)	211.06	49.74
	Summer	820	4.28 (4.52)	1.64 (2.12)	3.02 (2.15)	52.54	49.80
	Fall	820	9.44 (6.05)	4.49 (3.57)	4.97 (3.97)	91.89	30.49
	Winter	820	24.38 (7.59)	13.75 (6.41)	8.49 (5.79)	187.02	64.48
SC	Spring	1125	5.27 (3.79)	1.60 (1.38)	2.20 (2.03)	143.60	42.03
	Summer	1124	1.94 (1.88)	0.56 (0.63)	1.77 (1.73)	40.26	68.33
	Fall	1125	2.84 (2.17)	0.97 (0.78)	2.20 (2.31)	46.96	56.34
	Winter	1125	11.01 (4.71)	3.95 (2.21)	3.24 (3.39)	241.40	48.83
SB	Spring	408	5.65 (3.75)	2.04 (1.44)	2.56 (1.55)	129.04	36.98
	Summer	420	1.71 (1.20)	0.58 (0.43)	2.14 (0.99)	32.91	73.01
	Fall	418	4.91 (3.45)	1.83 (1.38)	2.71 (2.15)	96.49	45.96
	Winter	403	18.47 (12.17)	8.78 (6.54)	3.43 (3.01)	438.87	160.21
SK	Spring	260	10.16 (6.06)	5.70 (3.85)	5.24 (3.74)	94.08	28.25
	Summer	260	7.45 (7.90)	3.02 (3.57)	3.41 (2.58)	126.90	43.06
	Fall	260	8.71 (6.59)	4.51 (3.69)	4.81 (3.62)	91.61	39.04
	Winter	260	13.51 (5.77)	7.70 (3.52)	6.68 (4.14)	105.18	36.27
JP1	Spring	204	5.01 (1.47)	2.25 (0.73)	3.58 (2.48)	53.34	42.50
	Summer	204	2.46 (1.06)	0.76 (0.33)	2.91 (1.98)	34.93	73.80
	Fall	204	4.58 (1.93)	1.89 (0.91)	3.57 (2.50)	41.01	48.68
	Winter	204	8.15 (3.04)	3.75 (1.56)	4.48 (3.07)	85.57	36.53
JP2	Spring	285	4.11 (3.32)	1.84 (1.78)	3.09 (2.96)	40.45	42.56
	Summer	286	2.40 (2.10)	0.85 (0.82)	2.64 (2.77)	30.22	68.04
	Fall	286	3.94 (3.34)	1.62 (1.66)	3.12 (3.17)	31.45	48.14
	Winter	279	6.20 (4.58)	2.74 (2.44)	3.92 (4.20)	63.79	41.80
Entire domain	Spring	15175	3.88 (5.70)	1.77 (3.10)	1.97 (2.43)	119.82	49.39
	Summer	15207	1.38 (2.41)	0.50 (1.00)	1.59 (1.72)	49.35	70.20
	Fall	15224	2.69 (4.12)	1.18 (2.19)	2.06 (3.05)	55.88	48.79
	Winter	14075	7.28 (8.89)	3.62 (5.54)	3.20 (4.79)	135.63	50.42

⁽¹⁾ The number of data; ⁽²⁾ Unit, $\times 10^{15}$ molecules cm^{-2} ; ⁽³⁾ Standard deviations of the distributions of tropospheric NO₂ columns

Table S2. Average tropospheric NO₂ columns, standard deviations and the ratios of the $\Omega_{\text{CMAQ,AK}}$ to the Ω_{OMI} , when the INTEX-B and REAS NO_x emissions were applied into China for January.

Region	Inventory for China	n ⁽¹⁾	$\Omega_{\text{CMAQ,AK}}$ ⁽²⁾	Ω_{OMI} ⁽²⁾	R= $\Omega_{\text{CMAQ,AK}} / \Omega_{\text{OMI}}$
CEC	INTEX-B	896	12.32 (9.35) ⁽³⁾	14.32 (9.00)	0.86
	REAS		8.31 (6.42)		0.58
CEC2	INTEX-B	820	11.43 (6.82)	8.05 (6.34)	1.42
	REAS		5.91 (4.36)		0.73
SC	INTEX-B	1125	2.80 (1.83)	2.98 (3.09)	0.94
	REAS		1.92 (1.51)		0.64
SB	INTEX-B	386	5.43 (4.63)	3.34 (2.55)	1.63
	REAS		2.26 (1.69)		0.68
SK	INTEX-B	260	7.29 (3.79)	6.70 (4.64)	1.09
	REAS		7.24 (4.47)		1.08
JP1	INTEX-B	202	3.80 (1.86)	4.35 (2.58)	0.87
	REAS		4.83 (2.92)		1.11
JP2	INTEX-B	192	2.81 (2.67)	4.68 (4.60)	0.60
	REAS		2.78 (2.49)		0.59
Entire domain	INTEX-B	12901	3.22 (5.38)	3.23 (5.14)	1.00
	REAS		2.24 (3.56)		0.69

⁽¹⁾ Number of data; ⁽²⁾ Unit, $\times 10^{15}$ molecules cm^{-2} ; ⁽³⁾ Standard deviations of the distributions of tropospheric NO₂ columns

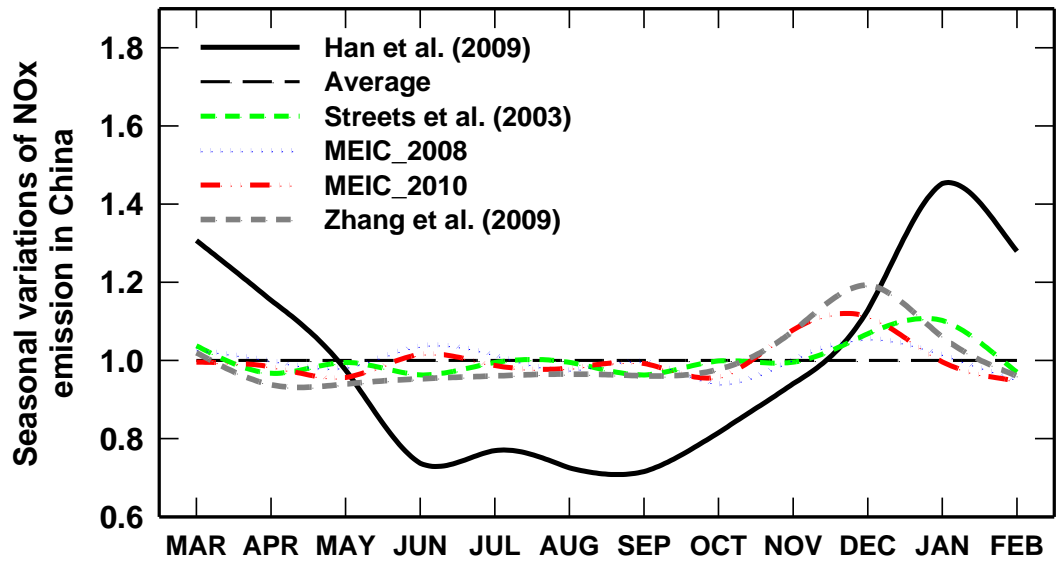


Fig. 1

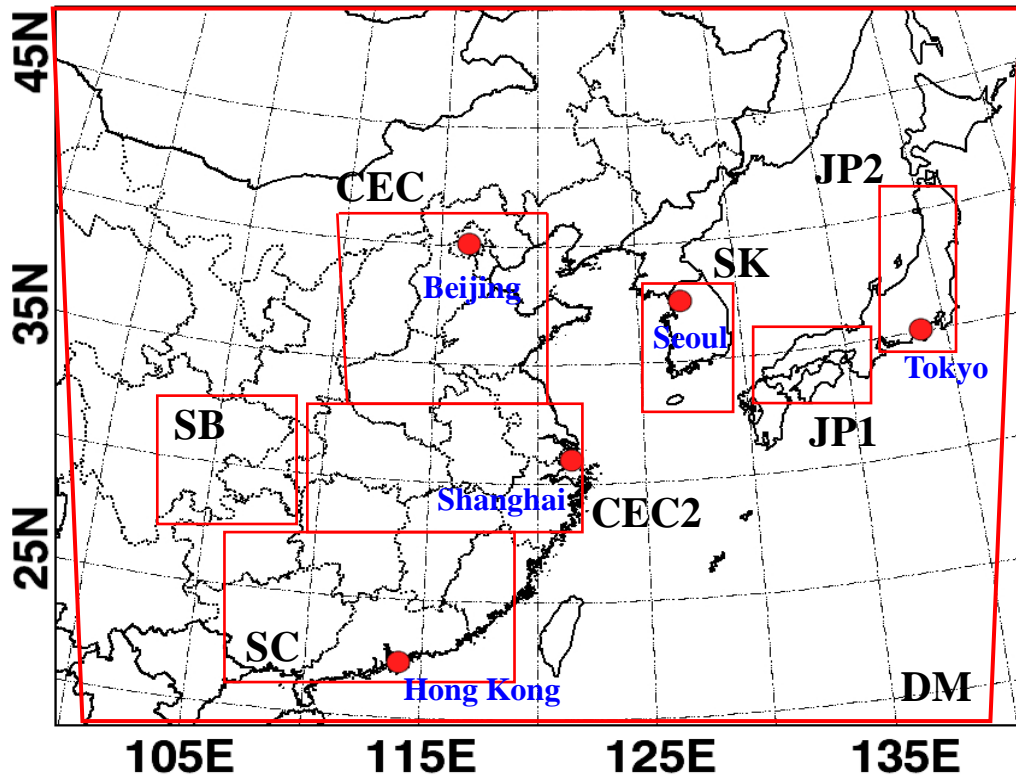


Fig. 2

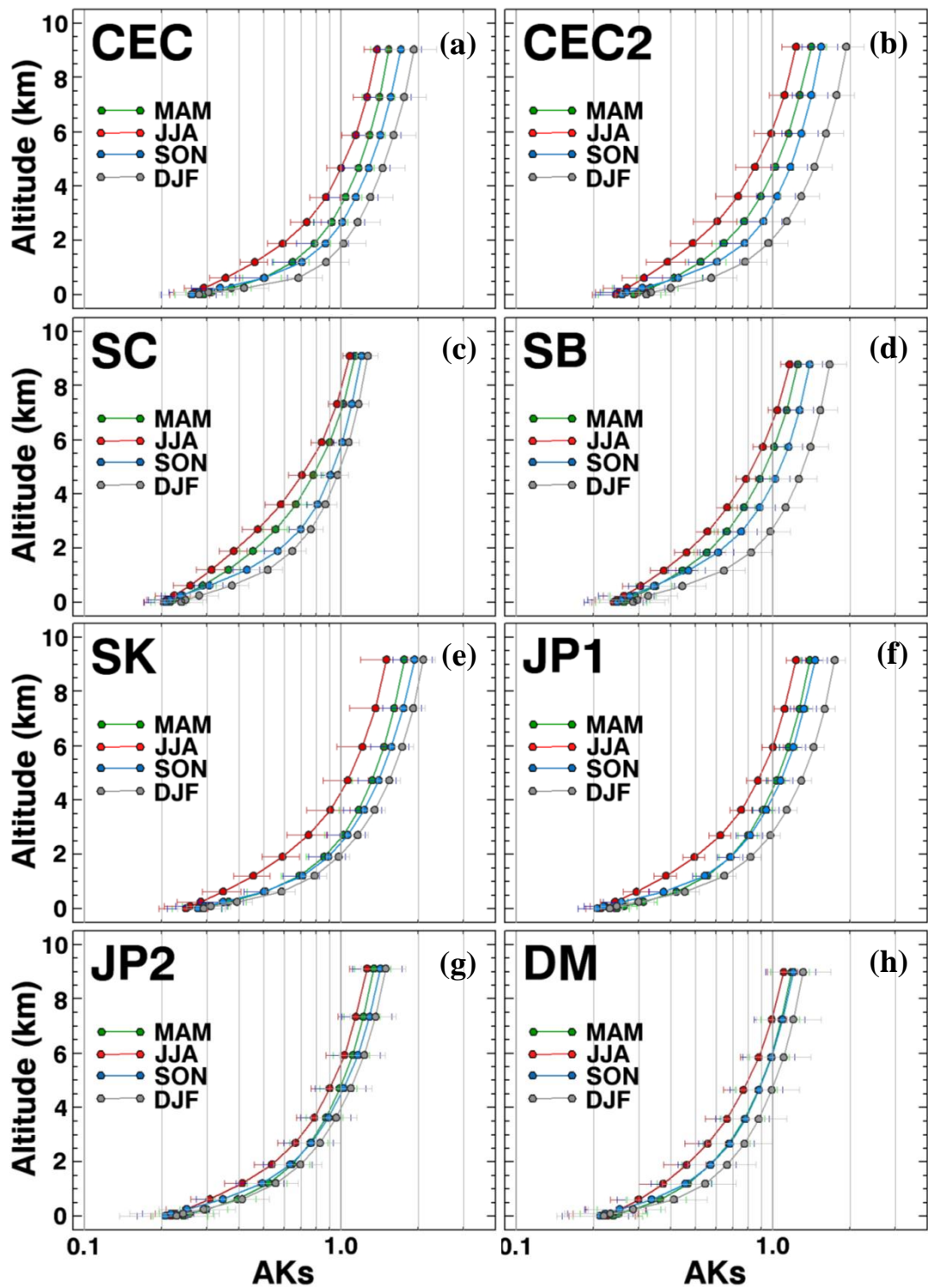


Fig. 3

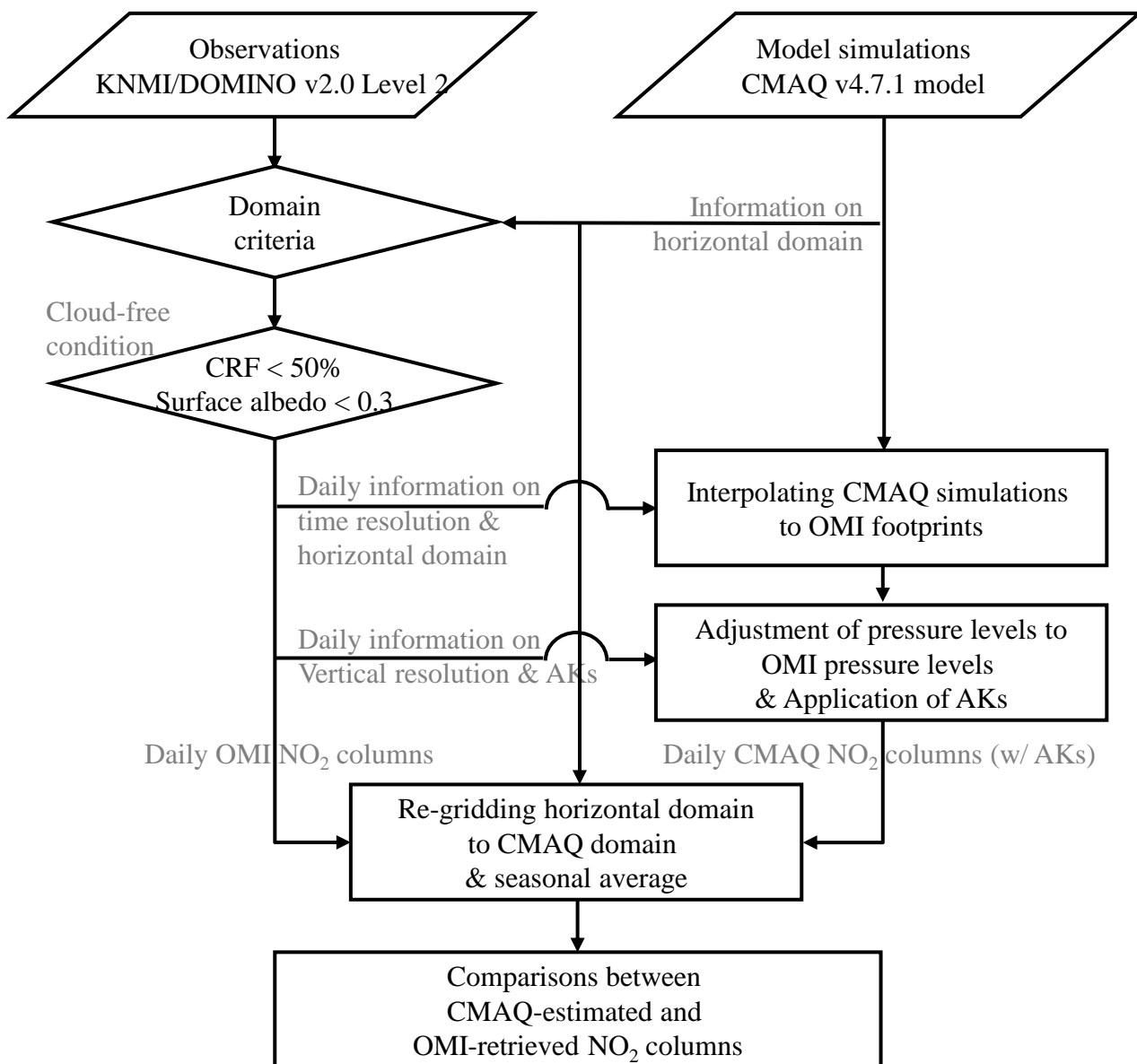


Fig. 4

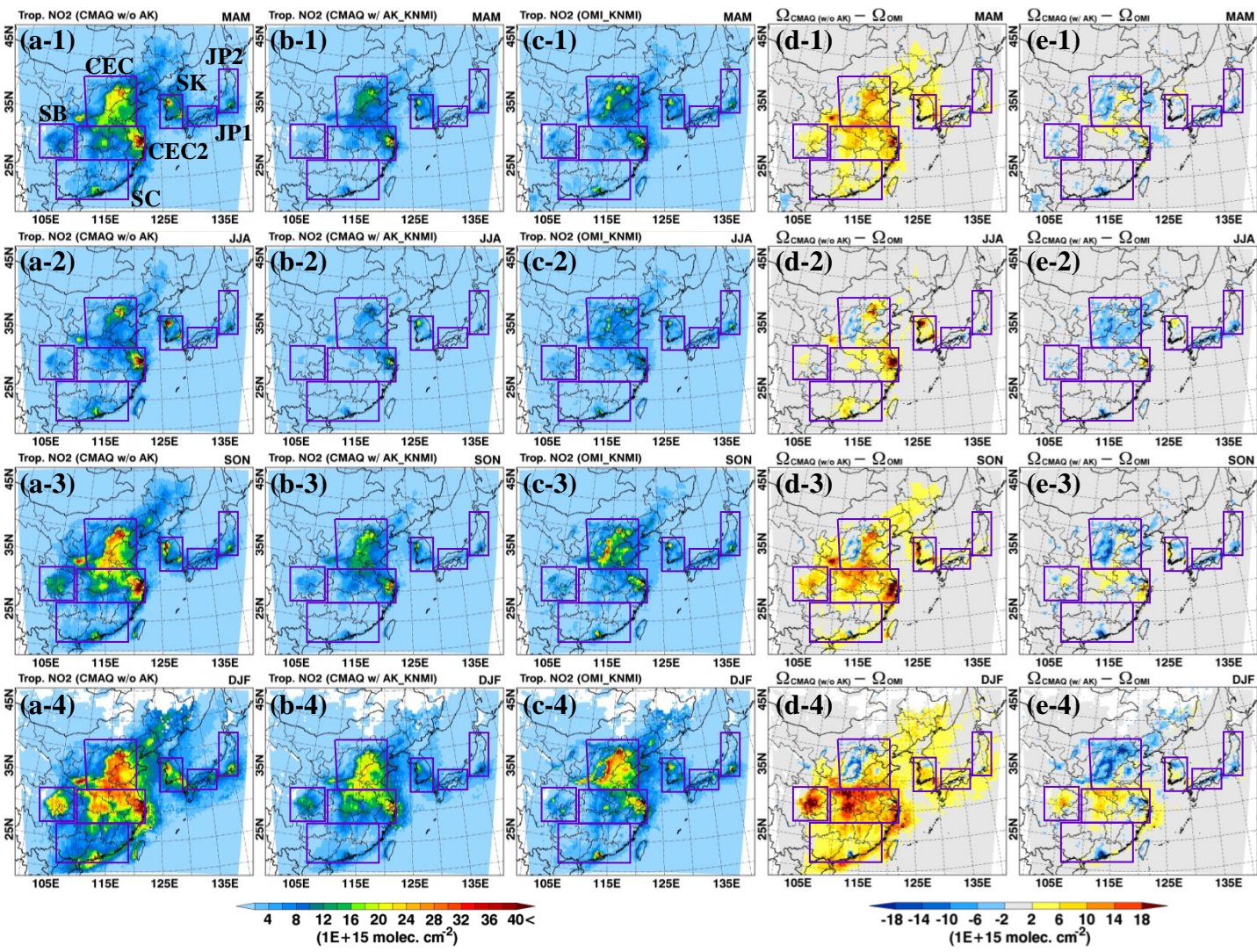


Fig. 5

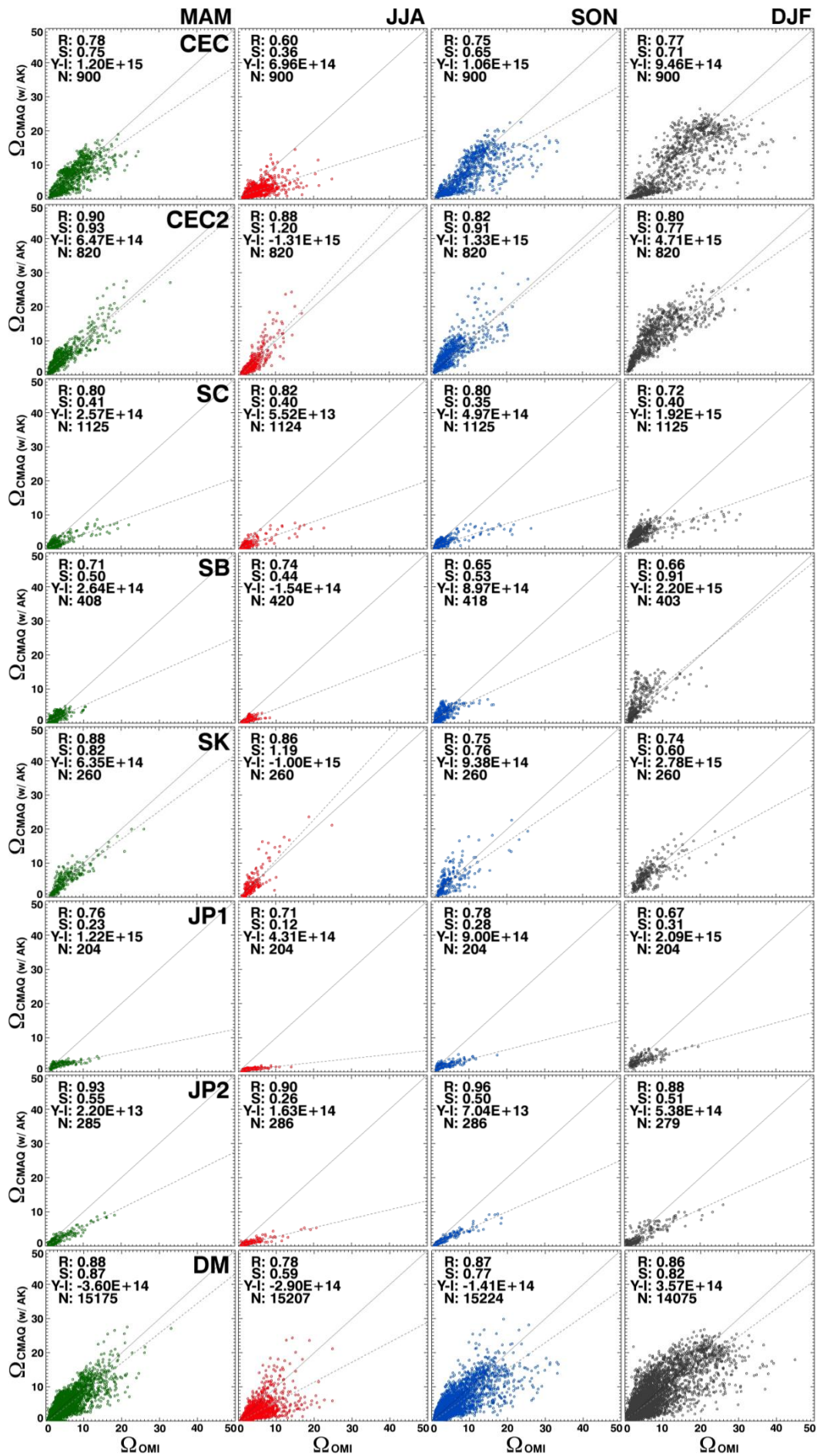


Fig. 6

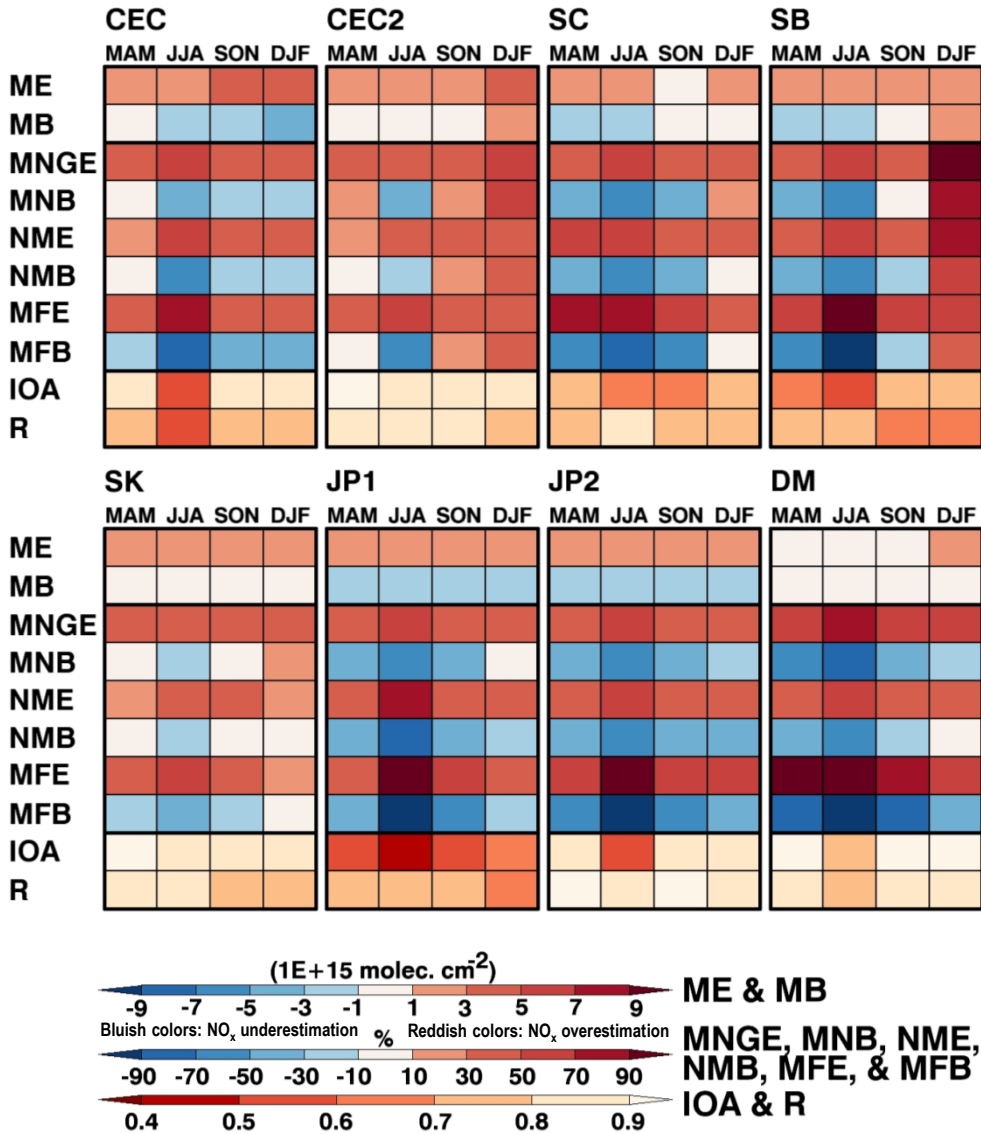


Fig. 7

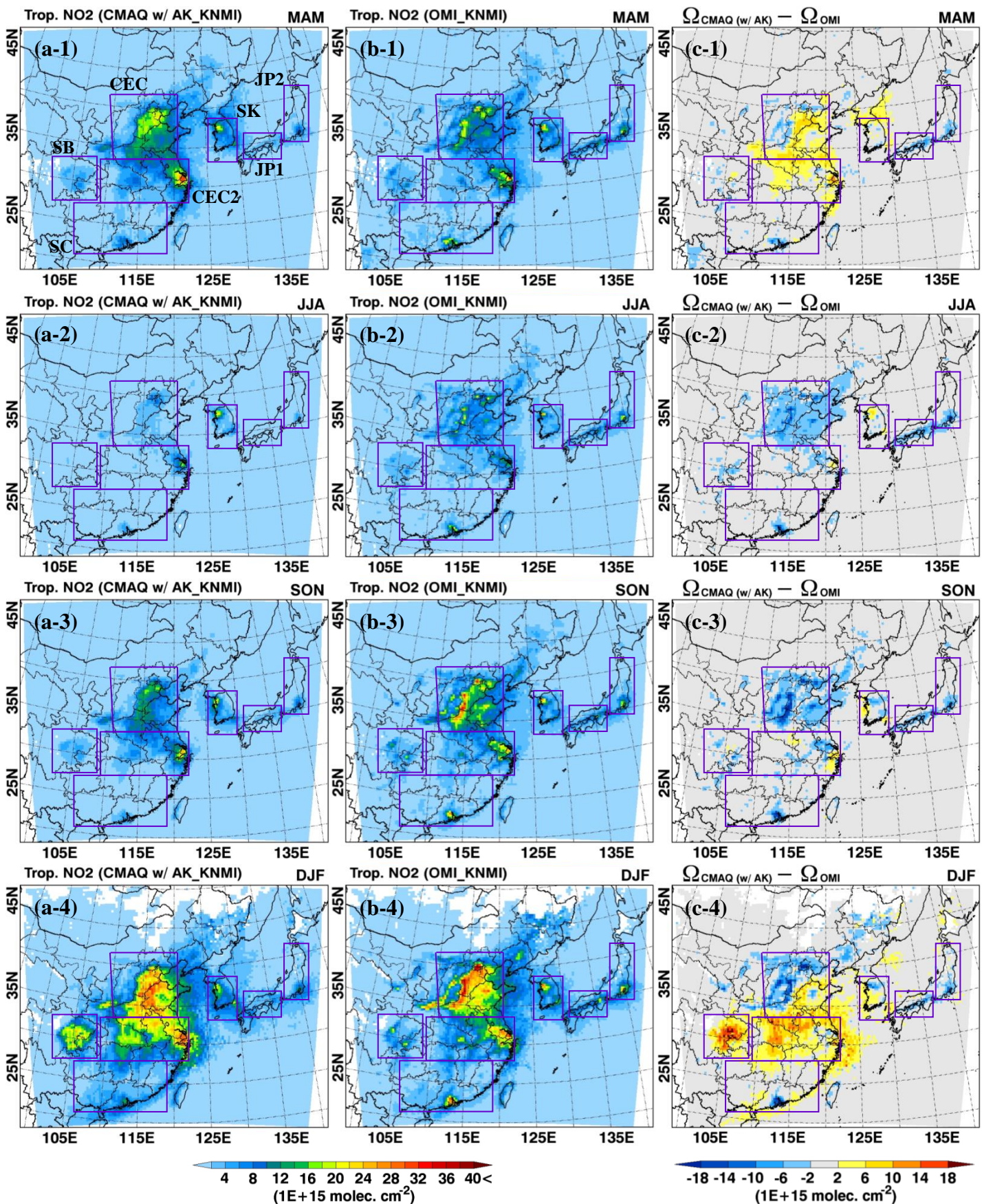


Fig. 8

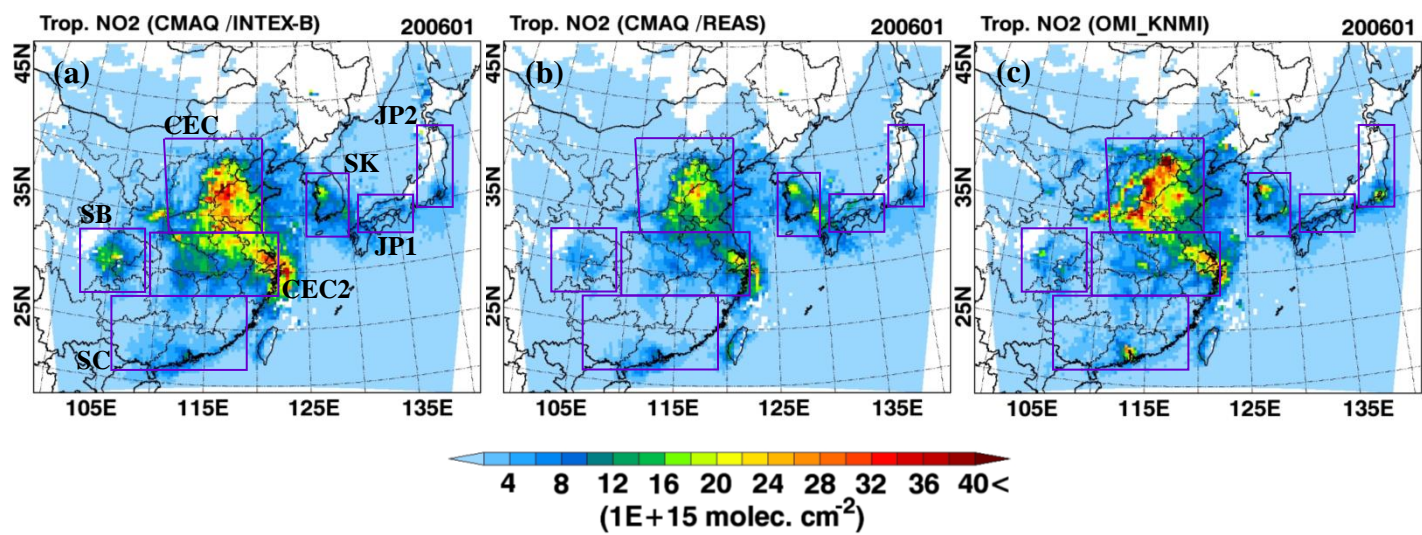


Fig. 9

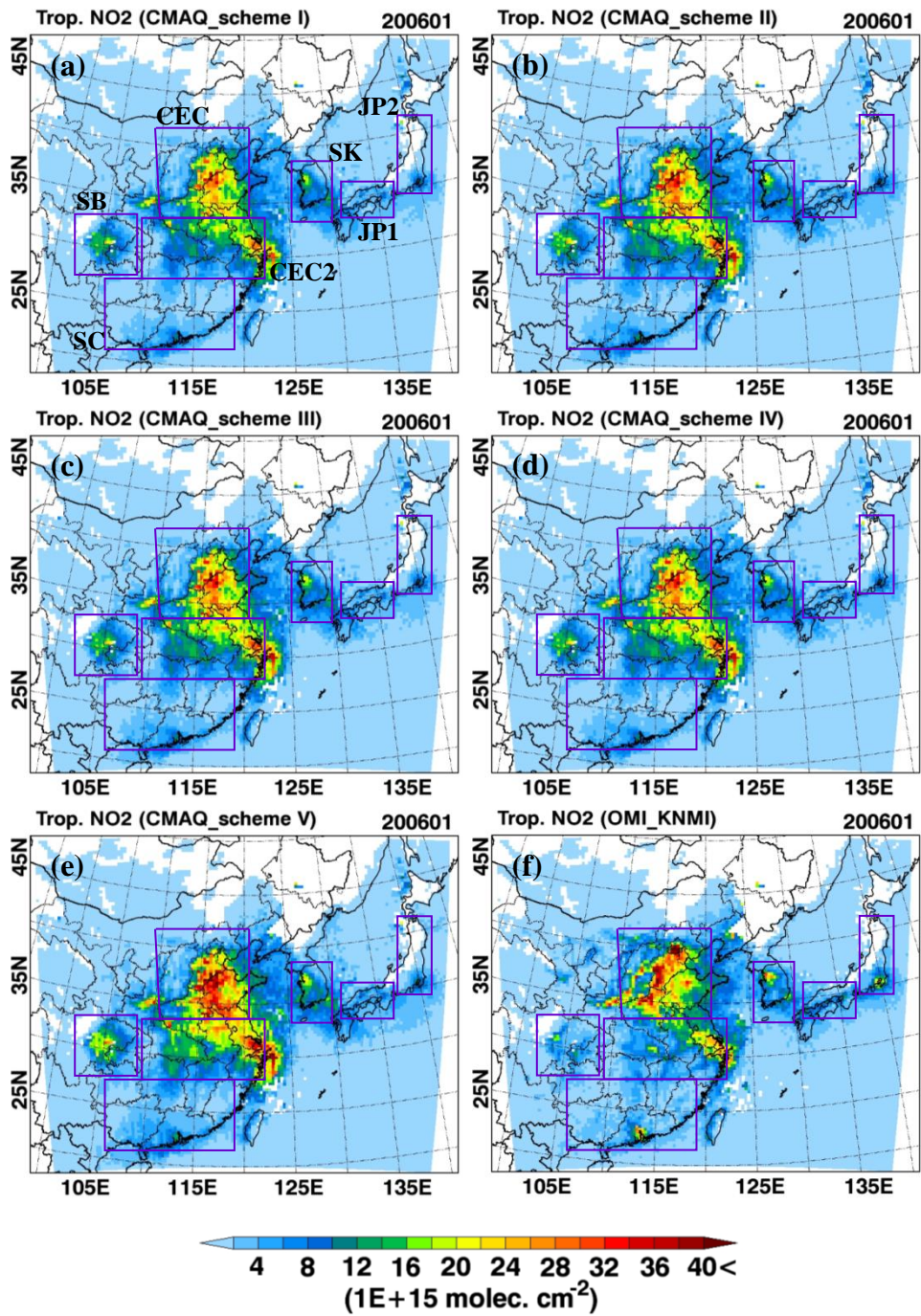


Fig. 10

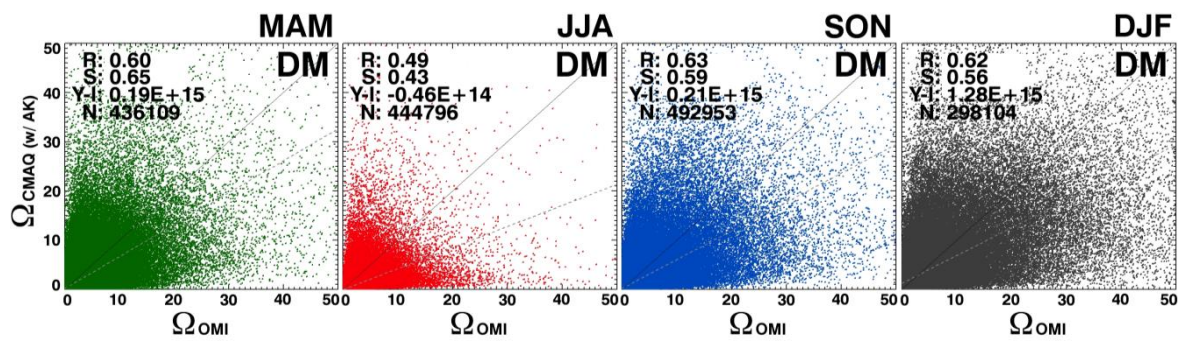


Fig. S1

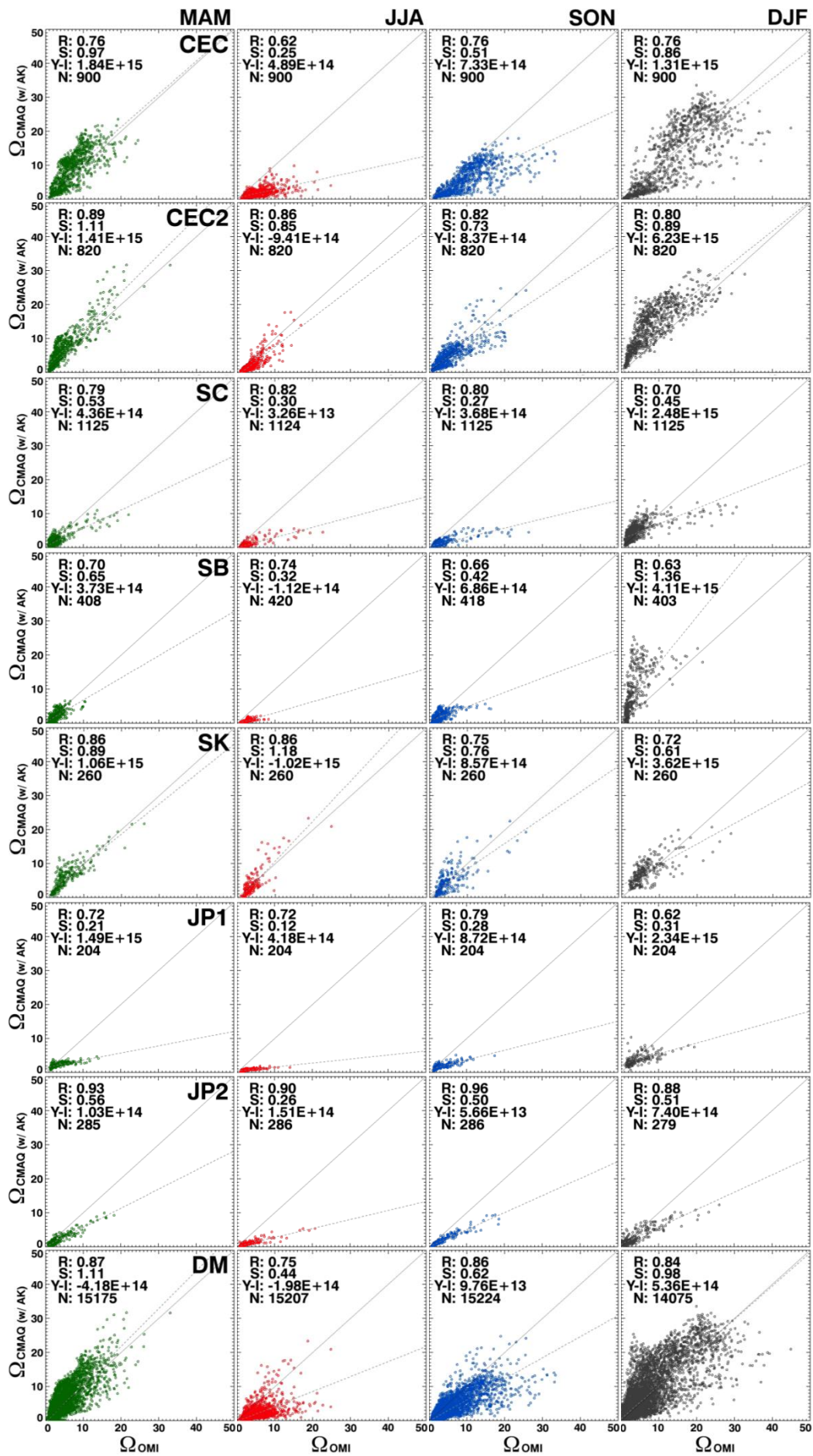


Fig. S2

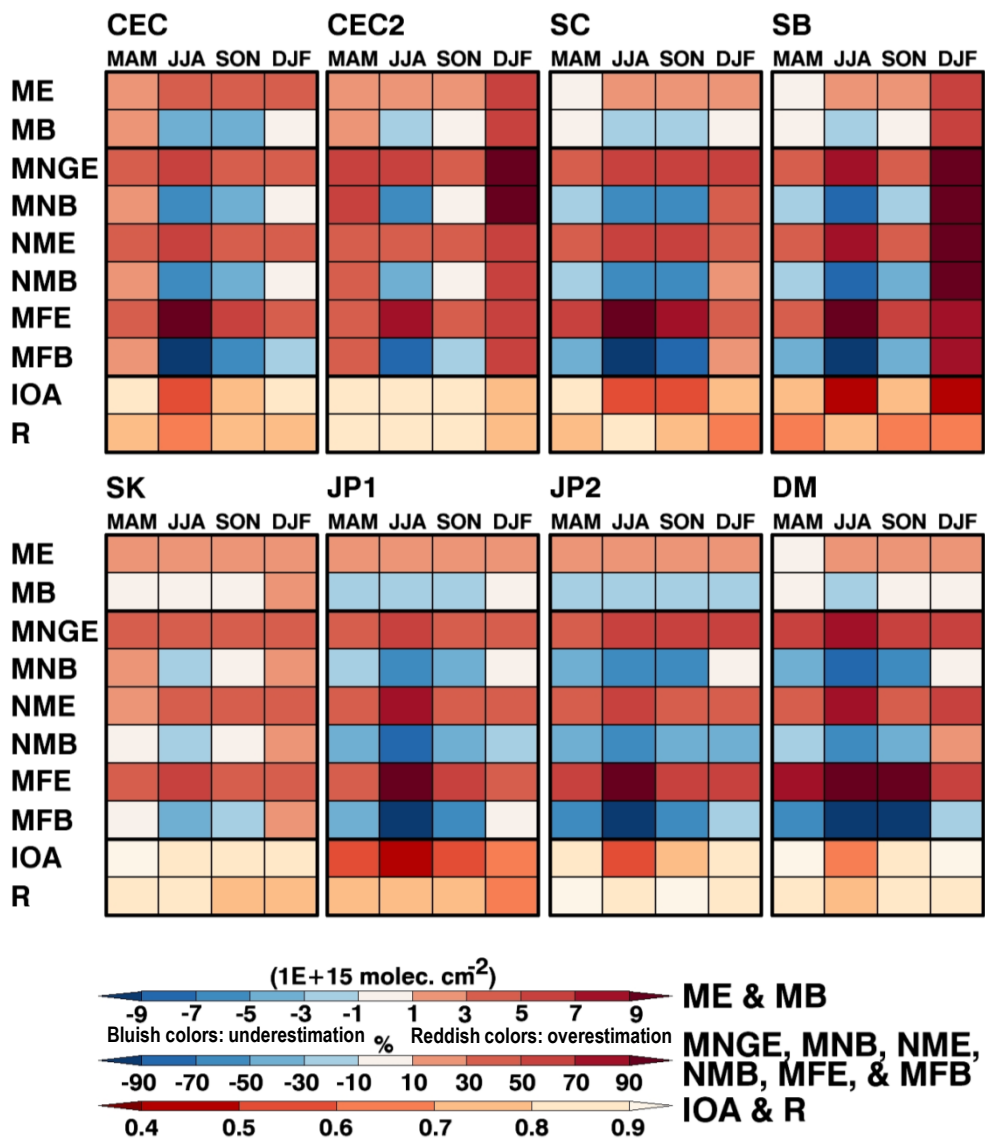


Fig. S3